Cumulus Momentum Transports in Tropical Cyclones

by
Cheng-Shang Lee

P.I. William M. Gray

Department of Atmospheric Science
Colorado State University
Fort Collins, Colorado

ONR No. N00014-C-0793

Colorado State University

Department of Atmospheric Science

Paper No. 341

CUMULUS MOMENTUM TRANSPORTS IN TROPICAL CYCLONES

by

Cheng-Shang Lee

Atmospheric Science Department

Colorado State University

Fort Collins, Colorado

80523

Atmospheric Science Paper No. 341

ABSTRACT

The net influence of sub-grid or smaller unresolvable scale processes (which cannot be directly detected from conventional observations) on the tangential momentum field in tropical cyclones has been calculated as a residual from the grid-scale momentum budgets of sixteen rawinsonde composite data sets. Results show that cyclone systems of the Pacific and Atlantic that are undergoing development have similar residual profiles in the vertical: positive cyclonic acceleration at upper and lower levels and negative cyclonic acceleration at between levels. Stronger systems have a greater magnitude of the sub-grid scale effect. These results are believed to represent primarily the cumulus convective transport (defined as cumulus friction). A simple cloud model is developed to diagnose momentum rearrangement in the vertical through mass recycling. Model results agree well with the residual calculations from the composites.

The total convective effect (TCE) on the tangential momentum includes the vertical transports by all the upward and downward motions which can be decomposed into the mean vertical motion and the local mass recycling. This TCE is found to reduce both the low level cyclonic and the upper level anticyclonic winds. These results imply that the net effect of the cumulus convective transport is down-gradient and acts to reduce the vertical wind shear of the cyclone. This mutual interaction between the cumulus convection and the larger scale flow features and their possible influence on tropical cyclone development is discussed.

TABLE OF CONTENTS

1. INTRODUCTION

The importance of cumulus convective processes on the horizontal momentum fields of tropical weather systems has been discussed by Gray (1967, 1973), Reed and Johnson (1974), Steven et al. (1977), Cho et al. (1979) and Shapiro and Stevens (1980). It is impossible to directly determine such convective influences because cumulus convection occurs on space and time scales significantly smaller than those in which measurements of the large-scale flow (defined here as that determined by a conventional rawinsonde observational network) patterns are taken. As a result, many investigators have tried to determine the residual of the large-scale momentum and vorticity budgets (Williams and Gray, 1973; Reed and Johnson, 1974; Shapiro, 1978; Cho et al., 1979 and Stevens, 1979). If cumulus convection is the only important small scale process, this residual may be considered to be largely contributed by the cumulus convective transport.

Theoretical cloud models have also been developed to diagnose the influence of cumulus convective transports on the large-scale dynamic fields (Austin and Houze, 1973; Reed and Johnson, 1974; Shapiro, 1978; Cho et al., 1979; Shapiro and Stevens, 1980). The model-diagnosed results are often compared with the calculated residuals of the large-scale budgets. A severe inconsistency between the model-diagnosed results and calculated residuals would throw doubt on any conclusions based on either the calculated residuals and/or model-diagnosed results. However, a reasonable consistency between these two would add support to both observational and model-inferred results and help support the hypothesis that cumulus convection is the most important small scale

process. Such results would also demonstrate that the calculated residual can well approximate the cumulus convective transport. These cloud models might also provide a framework for a parameterization scheme to represent cumulus convective transport in numerical models (e.g. Stevens et al., 1977; Fingerhut, 1982; Hack and Schubert, 1980).

Cumulus convection is typically observed to be quite substantial at the trough region of a tropical synoptic wave and at inner radii of tropical cyclone systems. Cumulus convective transports should therefore be both detectable in and important to the dynamics of these systems. Unfortunately, these weather systems typically exist over tropical oceans where conventional observations are limited. It is usually not possible to determine quantitatively the large-scale flow patterns (particularly the large-scale mean vertical motion) in individual case situations. One is obliged to composite many similar cases together to obtain quantitative and meaningful large-scale circulation patterns.

This composite technique has been used by Reed and Recker (1971) to study tropical synoptic waves over the western Pacific using 3 months of rawinsonde data. The data of the GARP (Global Atmospheric Research Project) Atlantic Tropical Experiment (GATE) have also been composited in the studies of tropical synoptic wave systems over Africa (Reed et al., 1977) and the eastern Atlantic Ocean (Thompson et al., 1979). The rawinsonde compositing at Colorado State University (CSU) has produced quite meaningful quantitative analyses of large-scale horizontal and vertical motion features of tropical cloud clusters and tropical cyclone systems (Williams and Gray, 1973; Frank, 1977a, 1977b; McBride, 1981; McBride and Zehr, 1981; and other papers).

Assuming that such composited large-scale motions are realistic, one may proceed a step further and ask the question: to what extent are the small (or unresolvable) scales of motion an important component to the necessary quantitative balances of the large (or resolvable) scales? To what extent can the large-scale momentum (also energy and moisture) budget be made without considering the smaller scale convective processes? The answers to these questions are of fundamental importance to the understanding and modeling of such convective weather systems.

Many efforts have been made to answer such questions for tropical waves using composite data (Reed and Johnson, 1974; Shapiro, 1978; Stevens, 1979; Cho et al., 1979 and Shapiro and Stevens, 1980). However, no one has yet performed such a study for the region of the tropical cyclone beyond the eye-wall. This paper thus attempts to answer the above questions for the inner $1\text{-}5^{o}$ latitude radius region of tropical cyclone systems - including tropical cloud clusters and hurricanes and typhoons.

To determine the cumulus momentum transport as a residual of the large-scale momentum budget, one is forced to evaluate the pressure gradient force which is usually less reliable. Therefore, most previous studies (mentioned above) have resorted to an analysis of the vorticity budget in which the pressure gradient force is not involved. However, these vorticity budget calculations include a twisting term which requires a knowledge of the horizontal gradient of vertical motion. This twisting term was neglected in the analysis of Reed and Johnson (1974). Shapiro (1978) calculated this term and suggested that this twisting effect is perhaps not important. Stevens (1979) also found that the twisting term was smaller than the other terms in the large-

scale vorticity budget equation. On the other hand, Cho et al. (1979) and more recently Yanai (private communication) have found that the twisting term is often very important in their analyses of tropical convection. These apparently contradicting conclusions indicate some general doubt in the reliability of the vorticity analysis. Such complication, however, will not arise in the present study which uses a cylindrical rather than a rectangular coordinate system.

In this study, the tangential momentum budget for the inner region (1-5° latitude radius) of tropical cyclone systems is considered rather than the vorticity equation. After taking an azimuthal average of the large-scale tangential wind equation, no knowledge of the height or pressure field is required because the pressure gradient term drops out in an integration around the vortex. No complicated twisting term is involved in the calculation of the residual.

The calculated residual, or the unresolvable part of the total vertical transport process, is defined as cumulus friction, denoted by cuF_θ (after Schneider and Lindzen, 1976; Stevens et al, 1977). Values of this cumulus friction for 16 composited tropical cyclone data sets are presented in Chapter 3. The consistencies and systematic variations between data sets are also discussed. In Chapter 4 these results will be compared with those diagnosed from a simple, single cloud model.

The total convective effect (TCE), which includes both the resolvable and the unresolvable parts of the vertical transport of tangential momentum, is also determined. Results are presented in Chapter 5. The mutual influences of the small scale convective systems and the large-scale momentum fields are also discussed.

2. RAWINSONDE COMPOSITE DATA SET

The rawinsonde composite data sets used in this study were established by Prof. W. M. Gray's tropical cyclone research group. They consist of 14 years (1961-1974) of northwest Atlantic and 10 years (1961-1970) of northwest Pacific rawinsonde soundings. Soundings are composited in a cylindrical coordinate system whose center is fixed on the cyclone center. Data are resolved into 7 radial, 8 azimuthal and 17 vertical grid points. Each grid point value on each level represents an area average over 2^{o} latitude radius and 45^{o} azimuth as shown in Fig. 1.

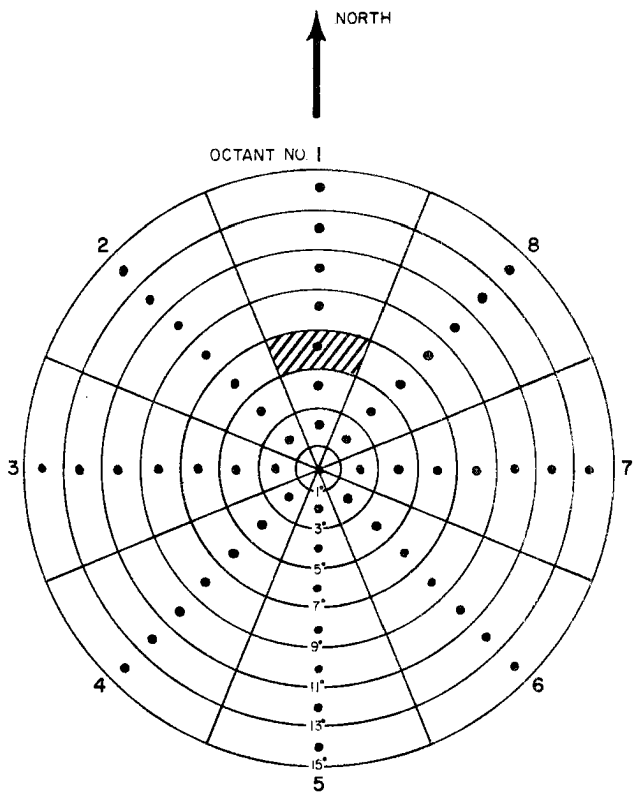

Fig. 1. Cylindrical grid for composite data. Arrow points toward north. The radial grid spacing is 2^{o} latitude. Each grid point value represents the average of all soundings in the grid box (shaded area).

The 16 composite tropical cyclones used in this study are summarized in Table 1. For a more complete description of these data sets, the Colorado State University (CSU) rawinsonde composite philosophy, and

TABLE 1

Summary of composite data sets used in this study.

NAME	DESCRIPTION	INTENSITY* STAGE	ESTIMATE OF MAX. SUSTAINED SURFACE WIND (m/s)	ESTIMATED CENTRAL PRESSURE (mb)	CENTER LATITUDE AND LONGITUDE	MOVING DIRECTION (toward) AND SPEED (m/s)		NO. OF SOUNDINGS INSIDE 15° RADIUS	COMMENT
ATLANTIC									
ATN1	Non-developing cloud cluster	1	$\lesssim$ 10	1010	20°N 80°W	281	3.8	3155	
ATN3	Non-developing depression	2	$\sim$ 15	1007	21°N 81°W	315	3.1	898	
ATD1	Prehurricane cloud cluster	1	$\lesssim$ 10	1007	18°N 72°W	289	4.9	714	
ATD2	Prehurricane depression	2	$\sim$ 15	1007	21°N 75°W	315	3.2	2168	
ATD3	Intensifying storm	3	$\sim$ 20	1000	22°N 78°W	325	3.1	2447	
ATD4(D)	Deepening hurricane	4-	$\sim$ 40		22°N 77°W	310	3.2	2881	Subset of ATD4
ATD4	Hurricane	4	$\sim$ 45	980	23°N 79°W	314	2.9	4721	

Table 1 (continued)

NAME	DESCRIPTION	INTENSITY STAGE*	ESTIMATE OF MAX. SUSTAINED SURFACE WIND (m/s)	ESTIMATED CENTRAL PRESSURE (mb)	CENTER LATITUDE AND LONGITUDE	MOVING DIRECTION (toward) AND SPEED (m/s)		NO. OF SOUNDINGS INSIDE 15° RADIUS	COMMENT
NORTHWEST PACIFIC									
WPN1	Non-developing cloud cluster	1	$\lesssim$ 10	1008	11°N 149°E	274	7.2	1961	
WPN3	Non-developing storm	3	$\sim$ 20	> 980 $\lesssim$1000	20°N 134°E	326	3.3	2071	
WPD2	Pretyphoon cloud cluster	1	$\lesssim$ 10	1005	10°N 153°E	286	5.0	2389	
WPD3	Intensifying storm	3	$\sim$ 20	1000	13°N 144°E	298	4.4	2660	
WPD3(D)	Deepening storm	3+	$\sim$ 20	> 980 $\lesssim$1000	17°N 142°E	301	3.8	2068	
WPD4(D)	Deepening typhoon	4-	$\sim$ 40		19°N 138°E	302	4.0	2584	Subset of WPD4
WPD4	Typhoon	4	$\sim$ 45	960	22°N 136°E	326	4.6	7756	
WPD4(F)	Filling typhoon	4+	$\sim$ 45		23°N 136°E	347	3.8	3384	Subset of WPD4
WPD5	Supertyphoon	5	$\sim$ 55	< 950 $\sim$	22°N 137°E	323	4.0	3001	Subset of WPD4

*Intensity stage: 1. cloud cluster 2. tropical depression 3. tropical storm
4. mature typhoon or hurricane 5. supertyphoon

specific composite techniques, the reader is referred to Williams and Gray (1973), Frank (1977a), McBride (1981), Gray (1981) and Gray et al. (1982).

2.1 Smoothing of the Composite Data

The composite data fields are considered to represent the average state of a tropical cyclone. However, it is inevitable that the composite average do include a degree of meteorological noise. To reduce this noise the smoothing routines contained in the SPLPAK package available from the National Center for Atmospheric Research (NCAR) were used. This package contains routines for fitting (by least-squares) a multi-dimensional cubic spline to values at specific points, and those for evaluating the spline at any point. A 2-dimensional (x and y-directions) cubic spline was used to smooth the composite data at each level. The degree of 'smoothness' depends on the number of nodes in each direction - the more nodes, the less smoothed the data. In order to choose an optimum degree of smoothness, the azimuthal average of the original composite tangential wind at 900 mb and 250 mb for the WPD4 data set and the smoothed tangential winds using 5-node and 9-node smoothing schemes were compared. The results are shown in Fig. 2. The five-node smoothing scheme used by Nunez (1982) is adequate for outer radii (defined as radius $> 5^{o}$ latitude) where the radial gradient is relatively weak; however, it is inadequate to resolve radial gradients at inner radii (defined as $1\text{-}5^{o}$ latitude radius). The 9-node smoothed data (used in this study) resemble the original data much more than the 5-node smoothed data at inner radii, which is the area of interest.

One of the advantages of using smoothing routines is the computation of horizontal gradient. Another advantage is that the value

at any point inside the smoothing domain can be interpolated. This provides a way of calculating the tangential wind change at each grid point due to storm motion. This is discussed in more detail in section 3.1. In addition, values at grid points with missing data can be objectively interpolated with a minimum of smoothing.

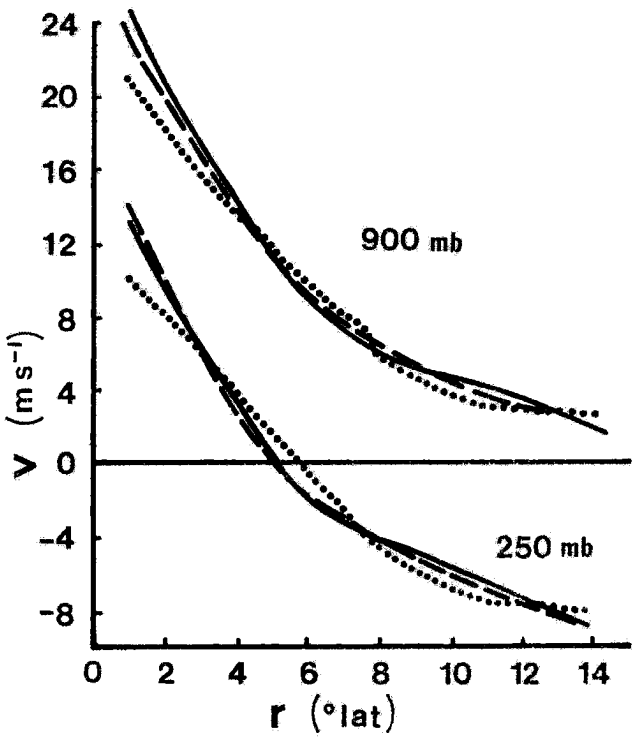

Fig. 2. Original (solid), 9-node (dashed) and 5-node (dotted) smoothed tangential wind field at 900 mb and 250 mb for WPD4 data set.

3. CUMULUS TRANSPORTS OF TANGENTIAL MOMENTUM (CUMULUS FRICTION) CALCULATED AS A RESIDUAL OF THE GRID SCALE BUDGET

Without the existence of cumulus convective systems, the small scale processes of the tropical cyclone would likely be of little importance compared to the large scale processes. However, in a tropical cyclone system with a horizontal scale of several hundred kilometers, there are many convective elements of horizontal scale of several kilometers or larger, which Arnold (1977) referred to as Basic Convective Elements (BCE). Figure 3 shows the BCE's associated with a mature tropical cyclone system. These convective elements often exist as line convection and frequently propagate at a speed greater than the environmental wind speed (Fujita and Black, 1970; Zipser, 1977). These convective systems transport heat, momentum and moisture vertically and horizontally in a manner which can be quite different from that of the larger, resolvable scale circulations. Therefore, large-scale dynamic and thermodynamic budgets computed only from the transports on the large or resolvable scale will probably be inadequate.

This paper attempts to determine how these small scale convective systems can affect the large scale momentum field in a tropical cyclone system. Two scales are thus defined: the grid (or large) scale and the sub-grid (or small) scale. Grid scale processes are those of horizontal scale equal to or greater than twice the grid spacing. Sub-grid scale processes have a horizontal scale smaller than twice the grid spacing. These sub-grid scale influences cannot be explicitly defined by our composite rawinsonde data but they can be calculated as a residual from the grid scale budgets.

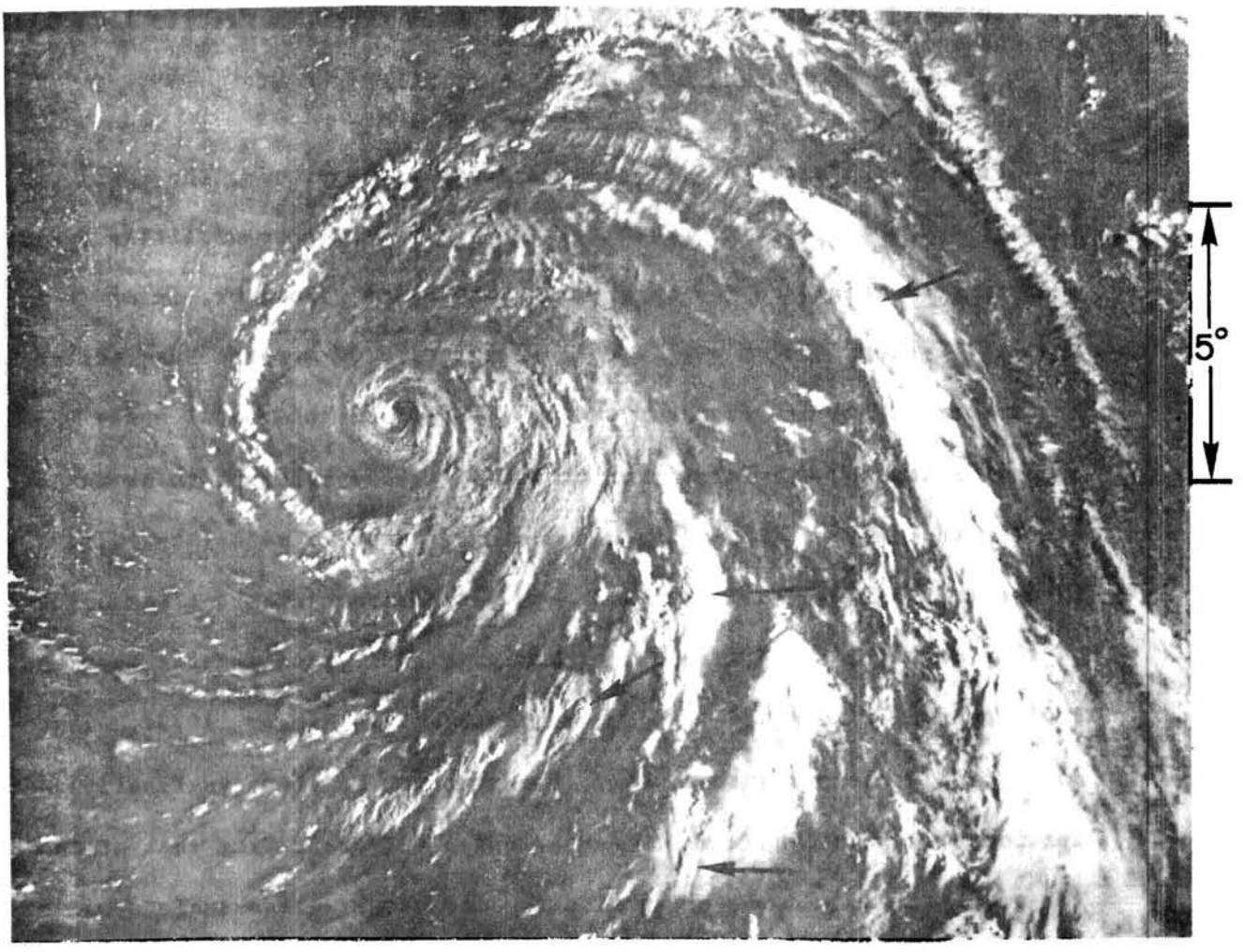

Fig. 3. Typhoon Wendy (8 September 1971, 2040Z) with individual basic convective elements (BCE's) indicated by arrows. (After Arnold, 1977).

3.1 Grid-scale Tangential Momentum Budget in Cylindrical Coordinates

The tangential wind equation in a geographically-fixed, cylindrical, isobaric coordinate system (r, θ, p) can be written as:

$$\frac{dv}{dt} = -\frac{1}{r}\frac{\partial \Phi}{\partial \theta} - fu - \frac{uv}{r} + SF_\theta \qquad [1]$$

where SF_θ is the tangential surface friction. (The usual symbol notation is used – see the list of symbol definitions in the rear of the paper.) Taking the grid box average of Eq. 1 gives, after some rearrangement:

$$\frac{\partial[v]}{\partial t} = -\frac{\partial r[u][v]}{r\partial r} - \frac{\partial[v][v]}{r\partial\theta} - \frac{\partial[\omega][v]}{\partial p} - \frac{\partial[\phi]}{r\partial\theta}$$

$$- f[u] - \frac{[u][v]}{r} + [SF_\theta] + [F_\theta] \qquad [2]$$

where brackets [ ] denote the grid point quantity which is implicitly the grid box average. The term $[F_\theta]$ is defined as the tangential friction due to all the sub-grid scale effects, or

$$[F_\theta] \equiv -\frac{[u'v']}{r} - \frac{\partial r[u'v']}{r\partial r} - \frac{\partial[v'v']}{r\partial\theta} - \frac{\partial[\omega'v']}{\partial p} + [x_p] \qquad [3]$$

where prime (') denotes the deviation from the grid box average and x_p is the sub-grid scale pressure gradient force, which is probably a result of convection-induced dynamic pressure.

The total vertical transport of tangential momentum associated with all the convective processes includes transport by the mean vertical motion, $(-\frac{\partial[\omega][v]}{\partial p})$, which can be determined directly from the composite data and that by vertical eddy processes, $-\frac{\partial[\omega'v']}{\partial p}$, which cannot be directly determined from the composite data. This eddy term, $-\frac{\partial[\omega'v']}{\partial p}$, should be important in the presence of convective systems and is defined as cumulus friction, denoted as $[CuF_\theta]$, following the nomenclature of Schneider and Lindzen, 1976; Stevens et al., 1977; and Fingerhut, 1982. However, this eddy term is not exclusively the result of cumulus convection. Any horizontal variation of vertical motion in a grid box is also included in this eddy term.

The most important sub-grid scale effect is often thought to be associated with the vertical eddy process, $-[\frac{\partial\omega'v'}{\partial p}]$. How the sub-grid scale pressure gradient force, x_p, can affect the large scale momentum fields is still not well understood. However, this pressure gradient

force should act in all directions and average out over a large area, and is thus neglected in this study (as in other studies). The first three terms on the right hand side of Eq. 3 are associated with horizontal sub-grid scale eddies, such as transient eddies, which may be of significant magnitude. This transient eddy effect will be discussed later.

Rearranging Eq. 2 gives:

$$[F_\theta] = \frac{\partial[v]}{\partial t} + \frac{\partial r[u][v]}{r\partial r} + \frac{\partial[v][v]}{r\partial\theta} + \frac{\partial[\omega][v]}{\partial p} + \frac{\partial[\phi]}{r\partial\theta} + f[u] + \frac{[u][v]}{r} - [SF_\theta] \qquad [4]$$

Except for the local time derivative of tangential wind and tangential surface friction, ($\frac{\partial[v]}{\partial t}$ and $[SF_\theta]$) , all the other terms on the right hand side of Eq. 4 can be evaluated by applying finite differencing on the composite data.

3.1.1 Local Change of Tangential Momentum

The local time derivative $\frac{\partial[v]}{\partial t}$ in a geographically-fixed coordinate system consists of two parts: one due to the motion of the system, denoted as $(\partial v/\partial t)_m$, and the other due to the intensity change of the system, denoted as $(\partial v/\partial t)_I$. Assuming that the system is in a steady state and moving with a mean speed (c) in a constant direction, the motion part can be rewritten as:

$$(\frac{\partial v}{\partial t})_m = - c \frac{\partial v}{\partial s} - \frac{c_\theta u}{r}$$

where $\partial/\partial s$ is the gradient along the direction of motion of the system and c_θ the tangential component of the cyclone speed. The right hand side of this equation is the tangential component of $(\vec{c}\cdot\nabla)\vec{V}$, where the arrow $\rightarrow$ represents a vector quantity. Smoothing routines have

been used to interpolate the value of v at points inside the composite grid where the data are not defined. This makes it possible to calculate $\partial v/\partial s$ at any grid point by using a finite difference scheme:

$$\frac{\partial v}{\partial s} = \frac{v(\Delta s) - v(-\Delta s)}{2\Delta s}$$

where $v(\Delta s)$ is the tangential wind speed at the point Δs distance ahead of the grid point, along the moving direction, and $v(-\Delta s)$ is the point behind.

To calculate the part due to intensity change of the system, $(\partial v/\partial t)_I$, the system is assumed to change its intensity to a later stage (see Table 2) in a certain time period, Δt. These time periods are determined by referring to those used by McBride (1979) and the typical rates of change of the maximum wind speed in tropical cyclones (Neal and Holland et al., 1978). Table 2 lists the time periods (Δt) between different intensity stages of a cyclone. The last line lists those storm systems assumed to be in steady state.

TABLE 2

Time period (Δt) for a system to intensify or weaken from an original stage to the later stage. Last line lists those data sets considered to have no intensity change.

Original Stage	Δt (days)	Later Stage
ATD1	1.5	ATD2
WPD2; ATD2	2.0	WPD3;ATD3
WPD3; ATD3	3.0	WPD4; ATD4
WPD4(D), WPD4(F); ATD4(D)	1.5	WPD4; ATD4
WPD3(D); ATN3	2.0	WPD4;ATN1
WPN1, WPN3, WPD4, WPD5, ATN1, ATD4		No Intensity Change

3.1.2 Surface Friction

Surface friction needs to be considered carefully in a momentum budget study and requires a knowledge of the surface stress and its vertical distribution. Many empirical formulae have been developed to calculate the surface stress (Garratt, 1977). However, none of these are applicable to the turbulent boundary layer of a tropical cyclone because of the unknown convective effect on the depth of the mixing layer and the breaking ocean wave condition associated with strong and gusty winds. However, over the 1-5^{o} latitude radius domain considered here these effects are assumed to be of secondary importance. Thus, following Frank (1977b) the Deacon bulk aerodynamic formula (Roll, 1965) is used to determine surface stress:

$$\tau_o = -\rho C_D | V_{10}| v_{10}$$

where $C_D = 1.1 \times 10^{-3} + 4.0 \times 10^{-5} |V_{10}|$ (V_{10} in m/s). $|V_{10}|$ and v_{10} are the total wind speed and tangential wind speed at 10 m height respectively. The wind speed at 900 mb is scaled by 0.8 to approximate the wind speed at 10 m height. In addition, a constant multiplier, 1.1 for Pacific data sets and 1.3 for Atlantic data sets, is used to adjust the surface stress calculated by the bulk formula, to account for the wind variation due to terrain effects which vary between the ocean basins. (There are more mountains around the Atlantic Ocean basin.)

The surface stress is assumed to vanish at 900 mb, which only allows the surface friction to be below this layer. Also, the surface friction is assumed to be larger at the surface and 950 mb than at 900 mb. However, no matter how the effect of the surface friction is

vertically distributed, its vertical integration (surface stress) is the same, that is,

$$\int_o^h SF_\theta \, dz = \int_o^h \frac{1}{\rho} \frac{\partial \tau}{\partial z} \, dz = \frac{1}{\rho} [\tau]_o^h = C_D |V_{10}| v_{10}$$

where h is the depth of the mixing layer and $\tau_h = 0$. (Density ρ is fairly constant in the mixing layer.)

3.2 Azimuthal Averaging of Grid-scale Tangential Momentum Budget

The sub-grid scale eddy effect $[F_\theta]$ at each grid point (shown in Fig. 1) can be calculated from Eq. 4 using composite rawinsonde data. However, these calculated residuals might have a magnitude of up to 50 m $s^{-1} day^{-1}$ especially at upper levels. These large and unrealistic values are primarily a result of the pressure gradient term in Eq. 4. The momentum budget study by Shapiro and Stevens (1980) had the same problem. This is the primary reason why other researchers have resorted to the use of the vorticity rather than the momentum equation. In a cylindrical coordinate system, however, the pressure gradient force term can be eliminated by taking the azimuthal average. When such azimuthal averaging is performed, Eq. 4 then becomes

$$\overline{[F_\theta]} = \overline{\frac{\partial [v]}{\partial t}} + \overline{\frac{\partial r[u][v]}{r \partial r}} + \overline{\frac{\partial [\omega][v]}{\partial p}} + \overline{f[u]} + \overline{\frac{[u][v]}{r}} - \overline{[SF_\theta]} \qquad [5]$$

where the overbar ($\bar{}$) denotes an azimuthal average. Note that this equation requires only observed wind data which are considered to be much more reliable than observed height data.

Taking azimuthal averages of Eq. 3 gives

$$\overline{[F_\theta]} = - \overline{\frac{[u'v']}{r}} - \overline{\frac{\partial r[u'v']}{r \partial r}} - \overline{\frac{\partial [\omega'v']}{\partial p}}$$

or

$$\overline{[F_\theta]} = -\frac{\overline{2[u'v']}}{r} - \overline{\frac{\partial[u'v']}{\partial r}} - \overline{\frac{\partial[\omega'v']}{\partial p}}, \qquad [6]$$

where the sub-grid scale pressure gradient ($[x_p]$) is also averaged out. Transient eddy effects, defined as $-\frac{\overline{[u'v']}}{r}$, are estimated by

$$-\frac{\overline{[u'v']}}{r} = \left(-\frac{\overline{u\,v}}{r}\right) - \left(-\frac{\overline{[u][v]}}{r}\right) \qquad [7]$$

where the product (u v) is calculated from each sounding. On the right hand side of Eq. 7, the first term, $-\frac{\overline{u\,v}}{r}$, represents the total effects due to the mean radial circulation, the standing eddy, and the transient eddy; the second term, $-\frac{\overline{[u][v]}}{r}$, represents the effects due to the mean radial circulation and standing eddy only, and has been included in Eq. 5.

Transient eddies have been determined from Eq. 7. They are generally small at inner radii but quite pronounced at outer radii especially at upper levels. For this reason, this study will evaluate the cumulus convective effects only at inner radii ($r < 5^\circ$ latitude) where the transient eddy effect does not greatly affect the results. Another reason for limiting this study within 5° latitude radius is the consideration of the generally observed radial extent of convection associated with a tropical cyclone system. (This will be discussed in the next section.)

Figures 4a and 4b illustrate the total effect, $-\overline{\frac{u\,v}{r}}$, and the mean and standing eddy effect, $-\frac{\overline{[u][v]}}{r}$, of 1-5° latitude radial and azimuthal averages for the typhoon (data set WPD4) and the hurricane (data set ATD4). The difference between the two profiles represents the transient eddy effect, $-\overline{\frac{[u'v']}{r}}$. This is generally insignificant except at 700 mb for WPD4 and at upper levels. The transient eddy effect term in Eq. 6 $(-\overline{\frac{2[u'v']}{r}})$ has a magnitude of about 3 m $s^{-1}day^{-1}$ or less at upper levels. Compared to the calculated residual $\overline{[cuF_\theta]}$ which has a magnitude of about 10 m $s^{-1}day^{-1}$ at upper levels (as will be shown later) this transient eddy effect can, to a first approximation, be neglected.

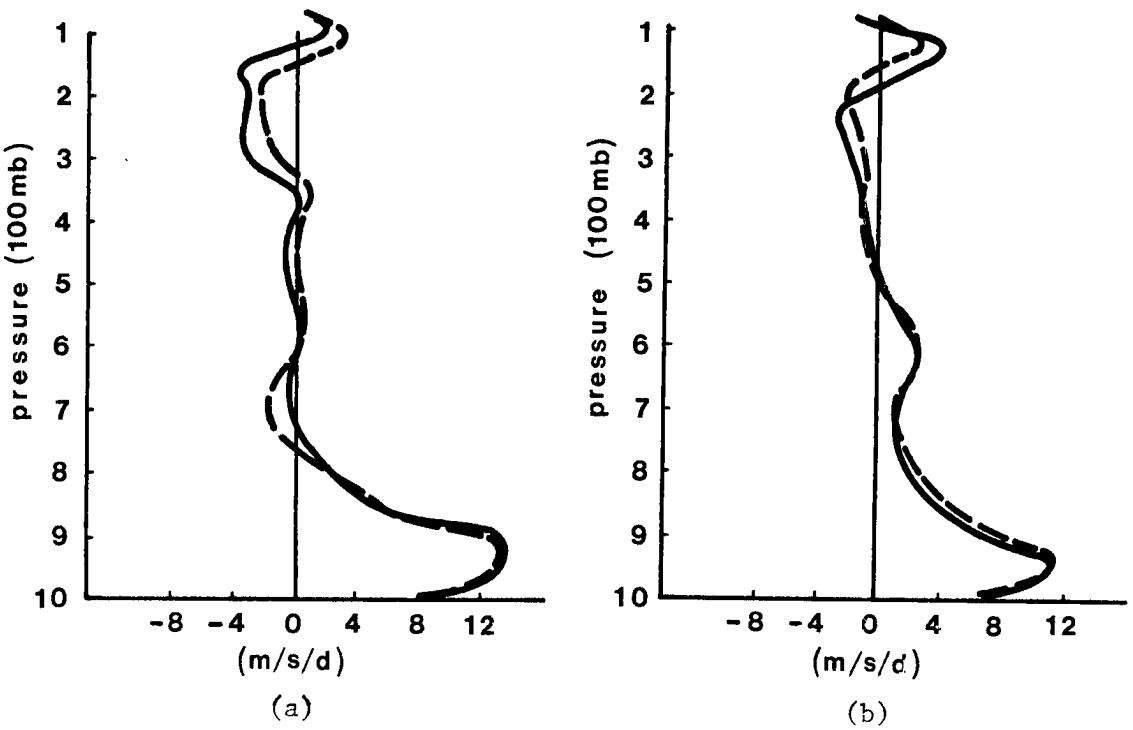

Fig. 4. 1-5° latitude radial averages of the total effect of $-\overline{uv}/r$, (solid), and mean and standing eddy effect, $-[u]\,[v]/r$, (dashed) for (a) typhoon (WPD4) and (b) hurricane $-[u][v]/r$ (ATD4) data sets.

Although the 1-5° averaged value of $\overline{[u'v']}$ can be quantitatively estimated from Eq. 7, the results are not accurate enough to provide a reliable estimate of the radial gradient term, $\overline{\frac{\partial [u'v']}{\partial r}}$. However, taking the 1-5° latitude radial average of this term yields $(\overline{[u'v']}_{5^\circ} - \overline{[u'v']}_{1^\circ})/4^\circ$. It is likely that this term has the same (or smaller) magnitude as that of $\overline{[u'v']}/r$ term, thus is probably negligible too. This term is thus assumed to be negligibly small.

After neglecting horizontal eddy effects $(-\overline{\frac{\partial [u'v']}{\partial r}}$ and $-\overline{\frac{2[u'v']}{r}})$, the cumulus friction can then be approximated by

$$\overline{[cu\ F_\theta]} \equiv -\overline{\frac{\partial [\omega'v']}{\partial p}}$$

$$\simeq \overline{\frac{\partial [v]}{\partial t}} + \overline{\frac{\partial r[u][v]}{r\partial r}} + \overline{\frac{\partial [\omega][v]}{\partial p}} + \overline{f[u]} + \overline{\frac{[u][v]}{r}} - \overline{[SF_\theta]} \qquad [8]$$

This quantity is termed the residual cumulus friction - cumulus friction calculated as a residual from the grid scale tangential momentum budget.

3.3 Calculated Residual - Cumulus Friction

Consideration of cumulus effects in a tropical cyclone requires an examination of the distribution of cumulus clouds. Besides the BCE's shown in Fig. 3, the radial extent of total cloudiness associated with different intensity stages of the tropical cyclone in the northwest Pacific in four cardinal directions is given in Table 3 (Arnold, 1977). The high standard deviations indicate a substantial variability in overall cloudiness. It must also be remembered that this mean radius may enclose large cloud-free regions. Nevertheless, these data show that most of the convection associated with the tropical cyclone occurs at radii inside of 5° latitude. Because very few observations are

TABLE 3

Radial extent of total storm associated cloudiness (after Arnold, 1977).

STORM STAGE	I		II		III		IV	
Mean Minimum Central Pressure (mb)	~1005		~998		~988		~959	
Direction:	Ave.	SD	Ave.	SD	Ave.	SD	Ave.	SD
North	4.6	2.1	3.9	1.5	6.1	2.0	5.3	2.2
East	5.6	2.7	5.2	2.1	5.9	2.7	5.7	2.5
South	5.1	2.8	4.7	2.9	6.5	3.1	5.8	2.5
West	5.0	2.6	3.5	1.8	5.2	2.3	4.9	1.8
R	5.0	2.6	4.3	2.2	6.0	2.6	5.5	2.3

Average (Ave.) and Standard Deviation (SD) values given in ^{o}Latitude.
R is the average radial extent of four cardinal directions.

available inside 1^{o} latitude radius, the residual cumulus friction being presented in this paper represents the $1\text{-}5^{o}$ latitude radial and azimuthal averages about the cyclone.

Assuming that cumulus clouds only rearrange horizontal momentum in the vertical, that is

$$\int_{P_{sfc}}^{100mb} \overline{[cu\ F_{\theta}]}\,dp = 0,$$

a correction factor must be applied at each level so that zero net tropospheric momentum change results. This correction factor is just the vertical mass-weighted average of the calculated residual (see section 3.4 for further discussion). The sign convention is that a

positive cumulus friction will cause a cyclonic acceleration (or anticyclonic deceleration) of the wind.

Figures 5 to 12 illustrate the vertical profiles of $1-5^{\circ}$ latitude radial and azimuthal averages of residual cumulus friction for all 16 data sets. Although these profiles may be somewhat in error due to the absence of horizontal eddies, uncertainty in the calculation of surface friction, noise inherent in the composite data, etc., they do show systematic variations between data sets and are believed to be reliable estimates of cumulus friction. For convenience, $1-5^{\circ}$ latitude radial and azimuthal averages will be omitted (but implied) in all the following discussions, unless otherwise mentioned.

Figure 5 shows the cumulus friction profiles for different stages of the developing tropical cyclone in the northwest Pacific. These profiles all have the same pattern: pronounced positive cumulus-induced acceleration at upper and lower layers, and negative acceleration at middle layers. The positive acceleration at 700 mb may be due to the transient eddy effect, $\frac{\overline{[u'v']}}{r}$ (refer to Fig. 4). However, the physical reason of causing these spikes is still not understood. These profiles also reveal that cumulus friction is directly related to system intensity. This is because the stronger weather systems have a larger vertical wind shear (and probably more vertical mass recycling) although not much difference exists in the mean vertical motion. The cumulus friction in the lower layers for Atlantic systems is not as positive as that for the Pacific cases (Fig. 6).

Figures 7 and 8 illustrate cumulus friction profiles for developing and non-developing cloud cluster systems. The two non-developing cases (WPN1, ATN1) exhibit a similar pattern: positive acceleration from the

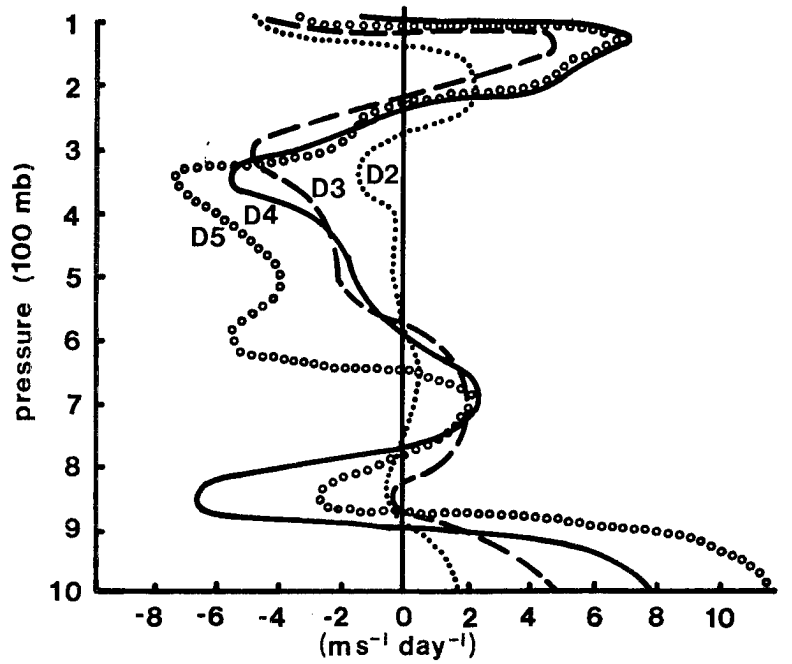

Fig. 5. 1-5° latitude radial and azimuthal averages of cumulus friction, [cu F_θ], for northwest Pacific (WP) developing tropical cyclone systems: a) WPD2 (cloud cluster), b) WPD3 (intensifying tropical storm), c) WPD4 (mature typhoon) and d) WPD5 (super typhoon).

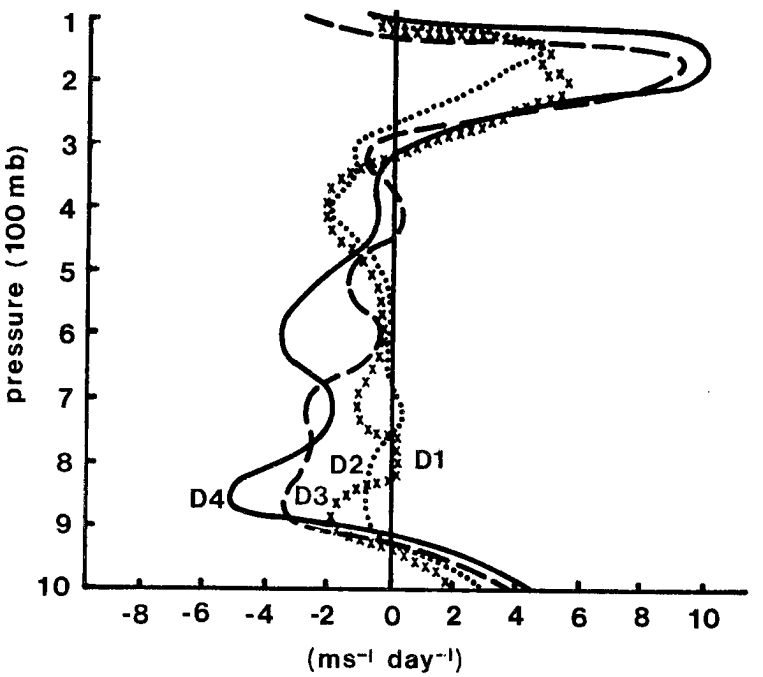

Fig. 6. 1-5° latitude radial and azimuthal averages of cumulus friction, [cu F_θ], for northwest Atlantic developing tropical cyclone systems: a) ATD1 (cloud cluster), b) ATD2 (tropical depression), c) ATD3 (intensifying tropical storm) and d) ATD4 (mature hurricane).

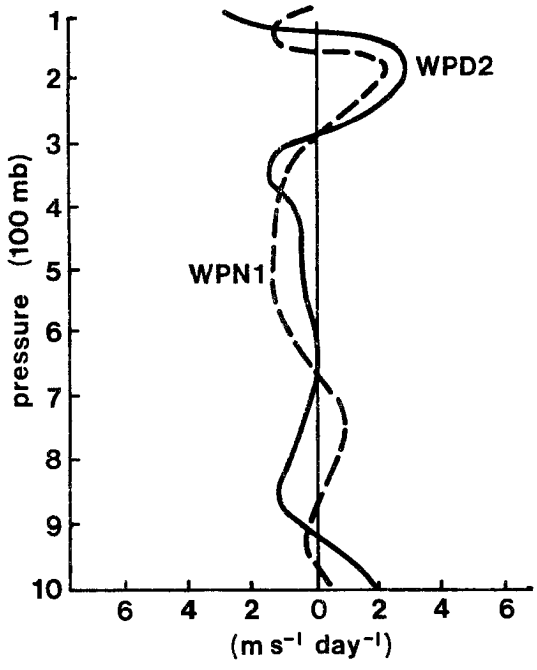

Fig. 7. The same as Fig. 5 but for developing (WPD2) and non-developing (WPN1) cloud clusters in the northwest Pacific.

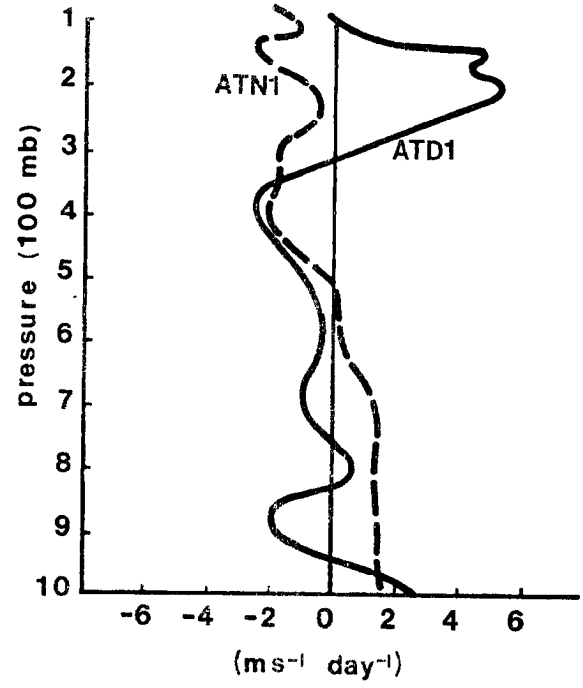

Fig. 8. The same as Fig. 5 but for developing (ATD1) and non-developing (ATN1) cloud clusters in the northwest Atlantic.

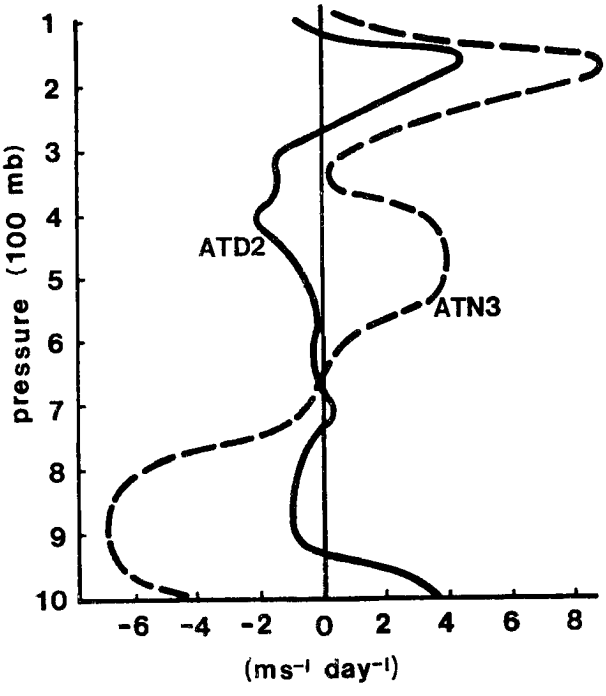

Fig. 9. The same as Fig. 5 but for developing (ATD2) and non-developing (ATN3) tropical depressions in the northwest Atlantic.

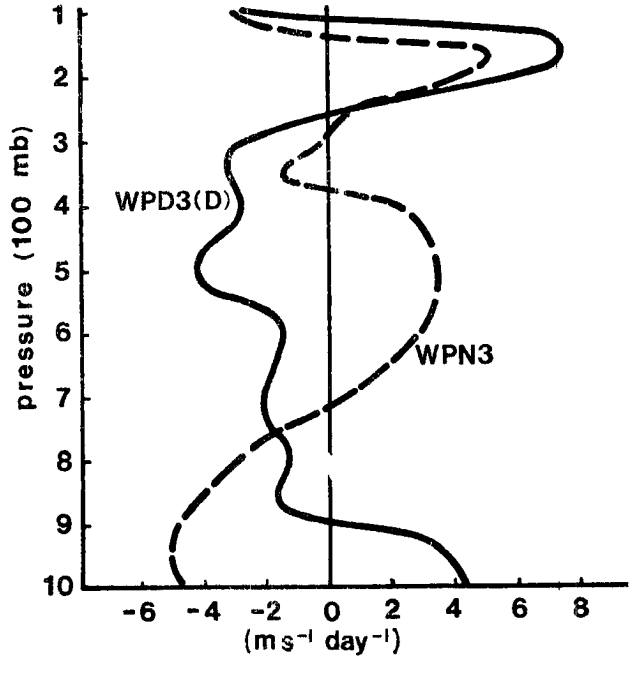

Fig. 10. The same as Fig. 5 but for deepening (WPD3(D)) and non-developing (WPN3) tropical storms in the northwest Pacific.

surface up to 600 mb (slightly negative at 900-950 mb for WPN1), and negative aloft except at 200-250 mb where cumulus friction is less negative or even positive (for WPN1). The two developing cases (WPD2, ATD1) also show a similar pattern which is qualitatively different from the non-developing cases. Although these differences are within the limits of possible error, they do show consistency for similar storm stratification in both ocean basins.

One might expect that the difference between the developing and non-developing cases would become larger as the system's intensity becomes stronger. Figures 9 and 10 show this progressive difference. For the intermediate systems of tropical depression (stage 2) or storm (stage 3) no apparent difference is found between the intensifying and non-intensifying cases at upper levels. Major differences do occur below 400 mb, however. Cumulus friction tends to increase the surface to 400 mb vertical wind shear for the intensifying cases and decrease greatly this vertical wind shear for the non-intensifying cases (ATN3, WPN3). For the mature typhoon and hurricane data sets (Figs. 11 and 12), cumulus friction increases the surface-350 mb vertical wind shear more for deepening cases (WPD4(D), ATD4(D)) than for filling/steady cases (WPD4, WPD4(F), ATD4). Also, the deepening cases have a smaller negative cumulus friction at 800-900 mb.

3.4 Discussion

Cumulus friction has been calculated as a residual of the tangential momentum equation for 16 composite data sets. Remarkable consistencies have been found between these profiles: Pacific versus Atlantic, strong versus weak; developing versus non-developing, etc. Although these profiles are considered to represent primarily cumulus

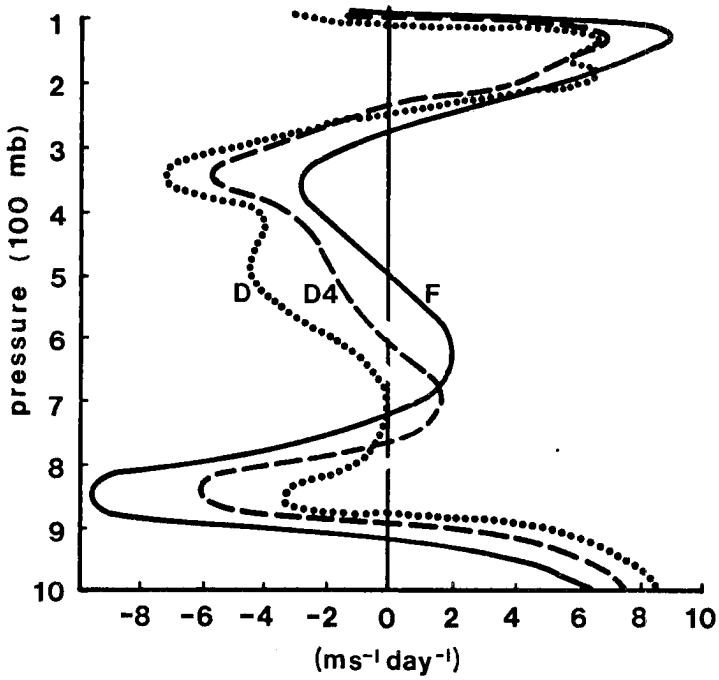

Fig. 11. 1-5° latitude radial and azimuthal averages of cumulus friction, $[\overline{cu}\ F_\theta]$, for mature (WPD4), deepening (WPD4(D)) and filling (WPD4(F)) typhoons in the northwest Pacific.

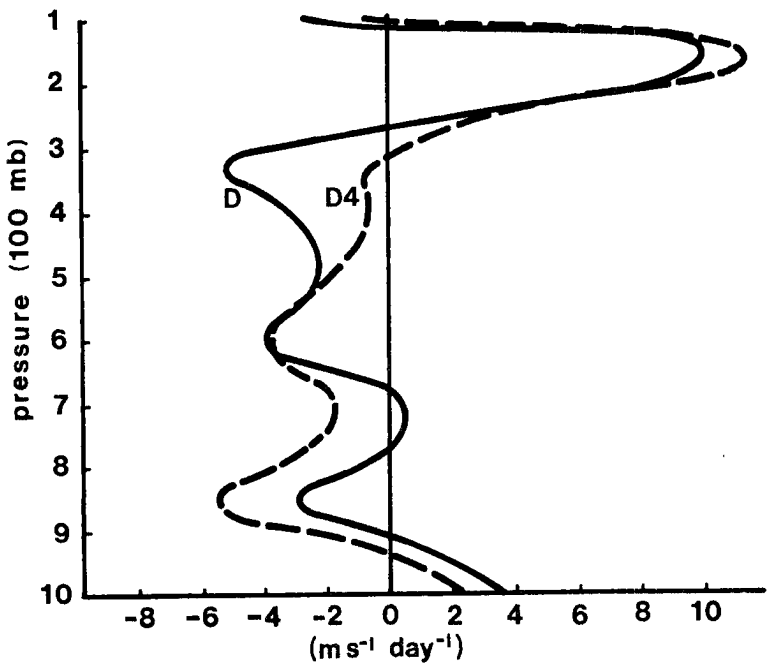

Fig. 12. 1-5° latitude radial and azimuthal averages of cumulus friction, $[\overline{cu}\ F_\theta]$, for mature (ATD4), and deepening (ATD4(D)) hurricanes in the northwest Atlantic.

friction, one has to remember that they may include other sub-grid scale effects.

Recalling that all these cumulus friction profiles have been adjusted to prevent any generation or destruction of tangential wind, cumulus convection is thus considered to be only a momentum rearrangement mechanism. The correction factor, which is subtracted out from the directly calculated residuals, represents the vertical mass-weighted average of momentum source or sink if momentum generation or destruction is present (a positive correction factor means a generation of cyclonic momentum). One might speculate that such generation of momentum is correlated to non-hydrostatic pressure gradient forces associated with the activity of squall line convection which somehow requires an environmental vertical wind shear. Figure 13 does show a positive correlation between the correction factor and the 900-200 mb vertical wind shear. However, this result needs more verification in other data sets and more theoretical backing before we can confidently conclude that cumulus convection can generate or destroy momentum. At this time the author believes it is more reasonable to treat cumulus convection as a vertical rearranging process only.

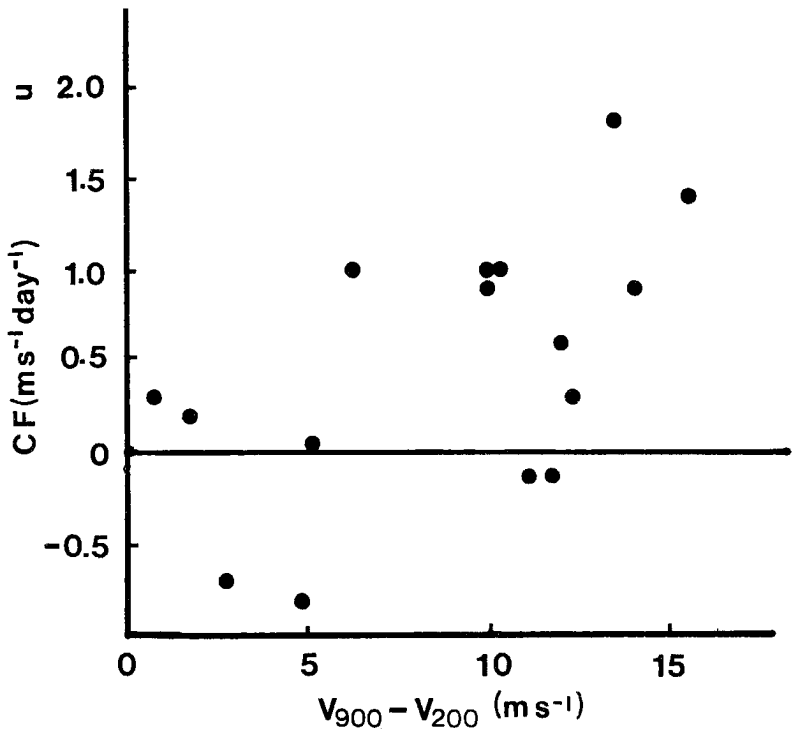

Fig. 13. The relationship between the vertical wind shear ($V_{900}-V_{200}$) and the correction factor (CF - vertical surface to 100 mb mass weighted average of unadjusted cumulus friction), which is subtracted out from the calculated residual to assure that the tropospheric average of cumulus friction is zero. Positive correlation is found between these two parameters.

4. PARAMETERIZATION OF CUMULUS FRICTION

Although the calculated residuals are considered to be reliable estimates of cumulus convective effects, they cannot be properly included in the governing equations without some parameterization scheme. To this end, many cloud models have been developed. Such cloud models treat the cumulus clouds as an ensemble and vary the entrainment and detrainment rates for different cloud types. Residual cumulus friction calculations are used to verify the cloud model diagnoses (Reed and Johnson, 1974; Shapiro, 1978; Cho et al., 1979; Shapiro and Stevens, 1980). In Shapiro and Stevens (1980), three cloud models are employed to diagnose the cumulus friction; they include spectral, bulk and single cloud models. They concluded that a single cloud model can reasonably well diagnose the sub-grid scale residuals (called apparent momentum source in their paper) for tropical waves in the Atlantic GATE region.

In this study, a simple single cloud model is developed to diagnose cumulus friction in the region $1-5^{o}$ latitude radius about the mature typhoon and hurricane. The model-diagnosed results are then compared to the residual cumulus friction presented in Chapter 3. Although a consistency between the calculated residual and the model-diagnosed cumulus friction may not provide a better understanding of mesoscale dynamics, it does give certain confidence as to how cumulus friction effects can be parameterized in numerical models. Because of our lack of knowledge of mesoscale dynamics, it is not necessarily true that a more complicated cloud model can handle this cumulus friction better than a simple model can. In addition, any consistency between the observed residual and the model results can be considered as general

support to the hypothesis that cumulus convective transports can be calculated as a residual.

4.1 Formulation

Total convective effect (denoted as TCE) is defined as including both vertical mean and eddy transports. This can be decomposed into upward and downward motion effects as:

$$\text{TCE} \equiv \left(-\frac{\partial[\omega][v]}{\partial p}\right) + \left(-\frac{\partial[\omega'v']}{\partial p}\right)$$

$$= \left(-\frac{\partial \omega_u v_u}{\partial p}\right) + \left(-\frac{\partial \omega_d v_d}{\partial p}\right) \qquad [9]$$

where subscripts u and d denote upward and downward motion respectively. Because the tropical atmosphere is so stable, all the upward motions have to be associated with cloud actions. For simplicity, a single cloud model might be utilized where the downward motion is considered to be the gentle broadscale subsidence having the same momentum as the environment. Equation 9 then becomes

$$\text{TCE} = -\frac{\partial \omega_c v_c}{\partial p} - \frac{\partial \omega_d v_e}{\partial p} \qquad [10]$$

where ω_c and ω_d are the average cloud and downward mass fluxes over a grid spacing respectively; v_c and v_e are the cloud and environmental momentums respectively. Values of ω_c, v_c, ω_d and v_e are taken to be constant at any level. Since $[\omega] = \omega_c + \omega_d$,

$$\omega_d = [\omega] - \omega_c. \qquad [11]$$

Also,

$$[v] = \sigma v_c + (1-\sigma) v_e \qquad [12]$$

where σ is the fractional area covered by cumulus clouds. If cumulus

clouds only occupy a very small fraction of the total area, i.e., $\sigma \ll 1$, Eq. 12 becomes

$$v_e \simeq [v]. \qquad [13]$$

Substituting (11) and (13) into (10) gives

$$TCE = -\frac{\partial}{\partial p}\left\{\omega_c v_c + ([\omega] - \omega_c)[v]\right\}$$

Thus,

$$TCE = \underbrace{\left\{-\frac{\partial[\omega][v]}{\partial p}\right\}}_{\text{mean convective effect}} + \underbrace{\left\{-\frac{\partial \omega_c (v_c - [v])}{\partial p}\right\}}_{\text{eddy convective effect}} \qquad [14]$$

and cumulus friction can be parameterized as

$$[cu\ F_\theta] \equiv -\frac{\partial[\omega' v']}{\partial p} \simeq -\frac{\partial \omega_c (v_c - [v])}{\partial p}$$

Or, taking the azimuthal average yields

$$\overline{[cu\ F_\theta]} = -\frac{\partial \omega_c (v_c - \overline{[v]})}{\partial p} \qquad [15]$$

It may, however, be inaccurate to assume that all the downward motions are in the form of gentle broadscale subsidence. Part of the downward motion might be in the form of strong cloud downdrafts or mesoscale downdrafts (Johnson, 1976, 1980; Zipser, 1977) which could conceivably carry upper level momentum down to the lower level. Then Eq. 9 should likely be rewritten as

$$TCE = -\frac{\partial \omega_u v_u}{\partial p} - \frac{\partial \omega_{dg} v_{dg}}{\partial p} - \sum_n \left(\frac{\partial \omega_{dn} v_{dn}}{\partial p}\right) \qquad [16]$$

where the subscript dg denotes the gentle subsidence, and dn any other kind of strong downdrafts. Through the same argument as before, Eq. 16 becomes

$$TCE = -\frac{\partial[\omega][v]}{\partial p} - \frac{\partial \omega_c (v_c - [v])}{\partial p} - \sum_n \frac{\partial \left\{ D_n \omega_d (v_{dn} - [v]) \right\}}{\partial p} \qquad [17]$$

and the azimuthal averaged cumulus friction becomes

$$\overline{[cu\ F_\theta]} = -\frac{\partial \omega_c (v_c - \overline{[v]})}{\partial p} - \sum_n \frac{\partial \left\{ D_n \omega_d (v_{dn} - \overline{[v]}) \right\}}{\partial p} \qquad [18]$$

where $D_n \equiv ([\omega_{dn}]/[\omega_d])$ is the fraction of total downward mass flux which is accomplished by the nth kind of strong downdraft. Equation 18 is identical to Eq. 15 if there is no other kind of strong downdraft present, i.e., $D_n = 0$. Note that in both Eqs. 15 and 18 the momentum carried down by gentle broadscale subsidence is assumed to be the same as the grid box average momentum [v] (Eq. 12). This assumption might not hold well at lower levels where the cumulus clouds might occupy up to 15–20% of the total area such that σ is not much less than one.

4.2 Moisture Budget and Vertical Mass Recycling

The determination of vertical mass recycling (or ω_c) is required to diagnose cumulus friction from Eqs. 15 and 18. Frank (1977c) employed a spectral cloud model and used the moist static energy (h) budget (first discussed by Yanai *et al.* (1973) and Lopez (1973)) to diagnose the vertical mass recycling, but strong downdrafts were not considered in these studies. Inclusion of cloud downdrafts or mesoscale downdrafts can cause important changes in vertical mass recycling (Johnson, 1976, 1980). To a large extent, the type of model to be employed determines the magnitude of the vertical mass recycling one obtains. In this study a single cloud model is employed, rather than a more complex spectral cloud model. This enables a simpler physical interpretation of the results.

Following Gray (1973) for a steady state cloud cluster system, the required upward moisture flux carried by the sub-grid scale circulation at any level k (k = 0 at surface) is given by:

$$(Q_r)_k = \{E_{sfc} \text{ or } (Q_r)_{k-1}\} - \{R_{\underline{k}} \text{ or } (C-E)_{\underline{k}}\}$$

$$\begin{Bmatrix}\text{Required upward moisture flux carried by local circulation at level k}\end{Bmatrix} \quad \begin{Bmatrix}\text{Surface evaporation (k=1) or } Q_r \text{ at level k-1 (k > 1)}\end{Bmatrix} \quad \begin{Bmatrix}\text{Condensation to rain or condensation minus reevaporation between level k and k-1.}\end{Bmatrix}$$

$$+ \{(\bar{\omega}\,\bar{q})_k - (\bar{\omega}\,\bar{q})_{k-1}\} + \{-(\overline{\nabla\cdot Vq})_{\underline{k}} \frac{\Delta p}{g}\} \qquad [19]$$

$$\begin{Bmatrix}\text{Vertical moisture convergence carried by mean vertical motion between level k and k-1.}\end{Bmatrix} \quad \begin{Bmatrix}\text{Horizontal moisture convergence between level k and k-1.}\end{Bmatrix}$$

where $\underline{k}$ denotes the layer between level k and k-1, and the overbar $(\bar{\ })$, denotes the mean circulation (or azimuthal average). Horizontal transport by transient eddies is neglected. The major problems in this calculation are the determination of surface evaporation and the amount of condensation that goes to rain at each layer.

4.2.1 Surface Evaporation

As discussed by Gray (1981) and Fingerhut (1982), use of the bulk-formula to calculate surface evaporation in the high wind speed condition of the tropical cyclone may result in a significant underestimation. If reasonably accurate rainfall data could be

obtained, it could be used to calculate surface evaporation as a residual from the formula

$$\begin{pmatrix}\text{Surface}\\ \text{evaporation}\end{pmatrix} = \begin{pmatrix}\text{Total}\\ \text{rainfall}\end{pmatrix} - \begin{pmatrix}\text{Total horizontal moisture}\\ \text{convergence from surface}\\ \text{to tropopause}\end{pmatrix} \quad [20]$$

where no net moisture change (in time) is assumed through the vertical column. Using rainfall observations from 16 hurricanes over Florida, Miller (1958) calculated rainfall amounts associated with hurricanes. Topographic effects were assumed to be negligible in these data due to the flat terrain of Florida. Measurement errors caused by high winds were also corrected. The rainfall amounts associated with typhoons have been obtained by Frank (1976) using the observed rainfall data from 13 small islands in the northwest Pacific. Figure 14 illustrates these rainfall amounts associated with hurricanes as well as typhoons. Very reasonable consistency is found between these two curves.

Using these rainfall data, the surface evaporations of mature hurricanes and typhoons at 1-5^{o} latitude radius about the system center are determined. Results are shown in Table 4. They are quite similar to those obtaned by Frank (1976) for the typhoon. These results also reveal that a typhoon system has almost the same surface evaporation as that of a hurricane system at 1-5^{o} latitude radius. The greater rainfall amount associated with the typhoon system is a result of larger horizontal moisture convergence.

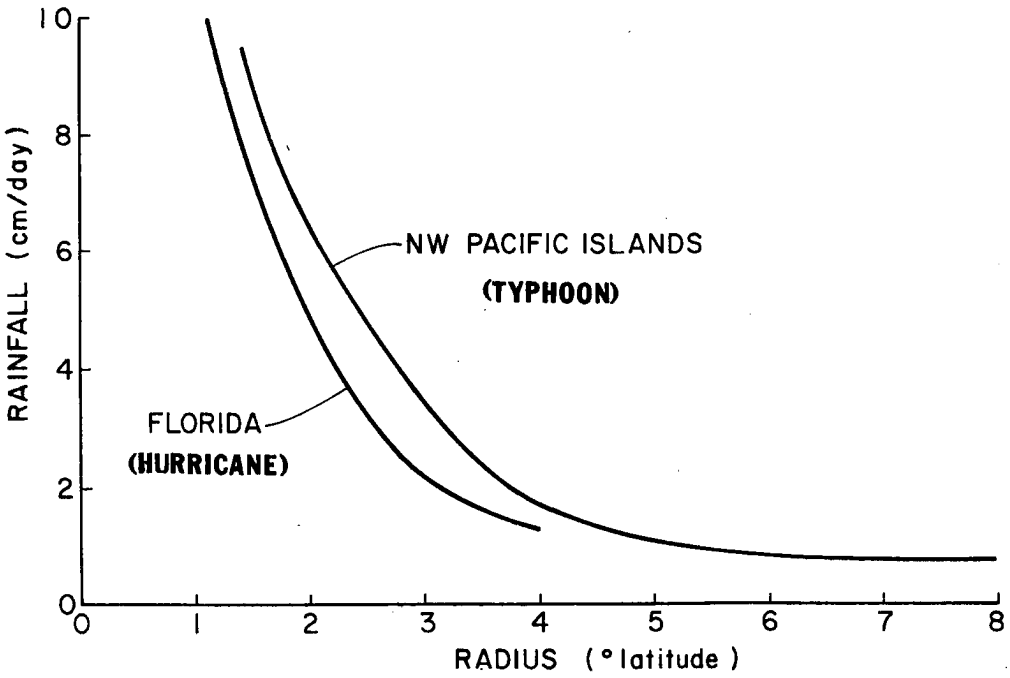

Fig. 14. Observed precipitation around tropical cyclones from Florida and from N.W. Pacific Islands (after Frank, 1976).

TABLE 4

Vertical integrated moisture budget associated with the typhoon and hurricane at 1-5° latitude radius about the system center in cm/day.

	Typhoon	Hurricane
Observed Rainfall	2.9	2.5
Horizontal Moisture Convergence	1.4	0.9
Required Surface Evaporation	1.5	1.6

4.2.2 Vertical Distribution of Condensation to Rain

An ad-hoc approach was used to determine the condensation to rain, or condensation minus re-evaporation (C-E), denoted as R at each layer. The rainfall R is decomposed into two parts, one part from mean vertical motion (R_m) and the other part from local recycling (R_r). The attempt here is to make the ratio of the local recycling (ω_r) to the mean vertical motion close to the ratio of recycling rainfall (R_r) to mean

vertical motion rainfall (R_m) at each layer or

$$(\omega_r/\bar{\omega})_k \simeq (R_r/R_m)_k$$

In addition, the resulting vertical mass fluxes have to resemble those obtained by Frank (1977c) when no strong downdrafts are considered.

The condensation due to mean vertical motion (C_m) can be calculated as:

$$C_m = -\left(\frac{\partial \bar{\omega}\,\bar{q}_s}{\partial p}\right)\frac{\Delta p}{g}$$

Assuming half of the liquid water condensed due to mean upward circulation is re-evaporated (E_m) then

$$R_m = C_m - E_m = 0.5\, C_m$$

or

$$(R_m)_{\underline{k}} = \frac{1}{2g}\left\{(\bar{\omega}\,\bar{q}_s)_k - (\bar{\omega}\,\bar{q}_s)_{k-1}\right\}$$

The total condensation to rain due to the local recycling ($(\sum_k R_r)_k$) can then be obtained as a residual by

$$\left(\sum_k (R_r)_{\underline{k}}\right) = (\text{Total rainfall}) - \left(\sum_k (R_m)_{\underline{k}}\right)$$

The vertical distribution of R_r is determined by the mixing ratio (q) and the difference between the saturation mixing ratio and the mixing ratio ($\Delta q = q_s - q$), or

$$(R_r)_{\underline{k}} = \frac{1}{2}\left\{\frac{(q\Delta p)_{\underline{k}}}{\sum_k (q\Delta p)_{\underline{k}}} + \frac{(\Delta q \Delta p)_{\underline{k}}}{\sum_k (\Delta q \Delta p)_{\underline{k}}}\left(\sum_k (R_r)_{\underline{k}}\right)\right\}$$

Therefore, the condensation to rain at each layer is

$$R_{\underline{k}} = (R_m)_{\underline{k}} + (R_r)_{\underline{k}}. \qquad [21]$$

The vertical distribution of R, R_m and R_r are shown in Table 5.

TABLE 5

Condensation to rain (mm/day) due to mean vertical motion (R_m), local recycling (R_r) and total upward motion (R) for the typhoon (WPD4) and the hurricane (ATD4) at 1-5° latitude radius about the system center.

	Typhoon (WPD4)			Hurricane (ATD4)		
Layer(mb)	R_m	R_r	R	R_m	R_r	R
100-200	0.07	0.03	0.1	0.03	0.02	0.05
200-300	0.73	.33	1.06	0.46	0.33	0.79
300-400	1.47	1.03	2.50	1.13	0.77	1.90
400-500	1.51	1.82	3.33	1.22	1.40	2.62
500-600	1.40	2.55	3.95	1.17	2.02	3.19
600-700	1.49	3.36	4.85	1.24	2.72	3.96
700-800	1.23	4.00	5.23	1.09	3.43	4.52
800-900	0.96	4.40	5.36	0.97	4.06	5.03
900-950	0.46	2.51	2.97	0.43	2.38	2.81
Total	9.32	20.03	29.35	7.74	17.13	24.87

4.2.3 Required Local Vertical Moisture Flux and Mass Recycling

Equation 19 then can be fully evaluated to determine the required vertical moisture flux. This is shown in Fig. 15 for the typhoon and the hurricane. It can be seen that these two curves are almost identical. The required vertical mass recycling (ω_{rk}) can be determined from (Gray, 1973)

$$(\omega_r)_k = -(Q_r)_k \, g/[(\overline{q_c})_k - (\overline{q_d})_k] \qquad [22]$$

where subscript u and d denote upward and downward as before. The upward cloud mass flux is given by:

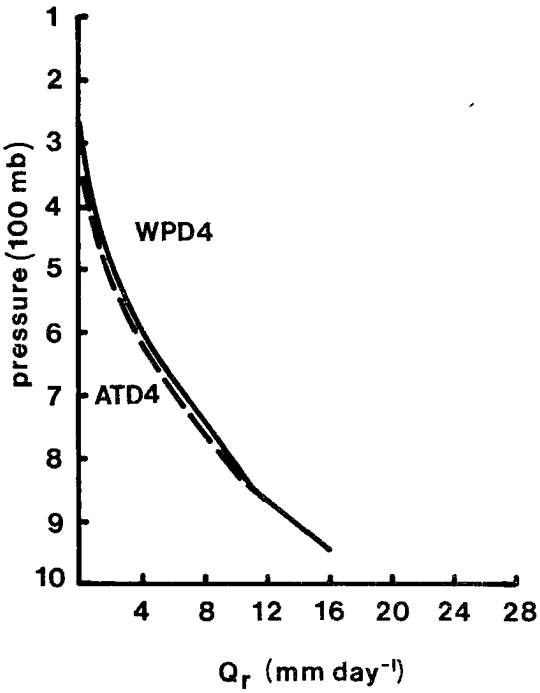

Fig. 15. Required vertical moisture flux carried by local circulation (Q_r) for WPD4 (solid) and ATD4 (dashed) data sets.

$$\omega_c = \bar{\omega} + \omega_r \qquad [23]$$

and the downward mass flux by:

$$\omega_d = -\omega_r \qquad [24]$$

The quantity $\bar{q}_{ck}$ can be approximated by $\bar{q}_{sk}$ (calculated from mean temperature) if all the upward motions are assumed to be saturated. This approximation is affected by two factors: 1) some upward motion might be sub-saturated and 2) a slightly higher temperature might be expected inside the convective clouds. However, these two effects will tend to cancel each other. If the downward motion is assumed to be in form of gentle subsidence, then by the same argument as that of the momentum, $\bar{q}_d$ can be approximated by $\bar{q}$. The profile of $(\bar{q}_c - \bar{q})$ is shown by the solid line in Fig. 16. The required local mass recycling was then calculated (see Fig. 17). The close similarity between the

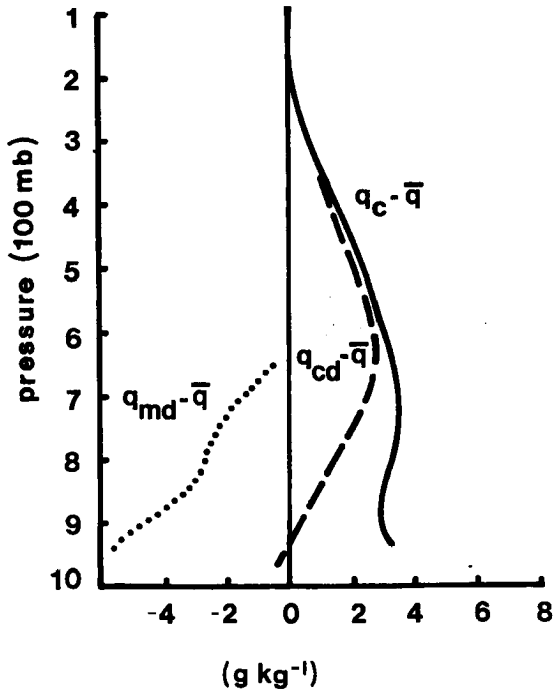

Fig. 16. Assumed mixing ratio anomalies for cloud updrafts ($q_c - \bar{q}$), cloud downdrafts ($q_{cd} - q$) and meso-scale downdrafts ($q_{md} - q$).

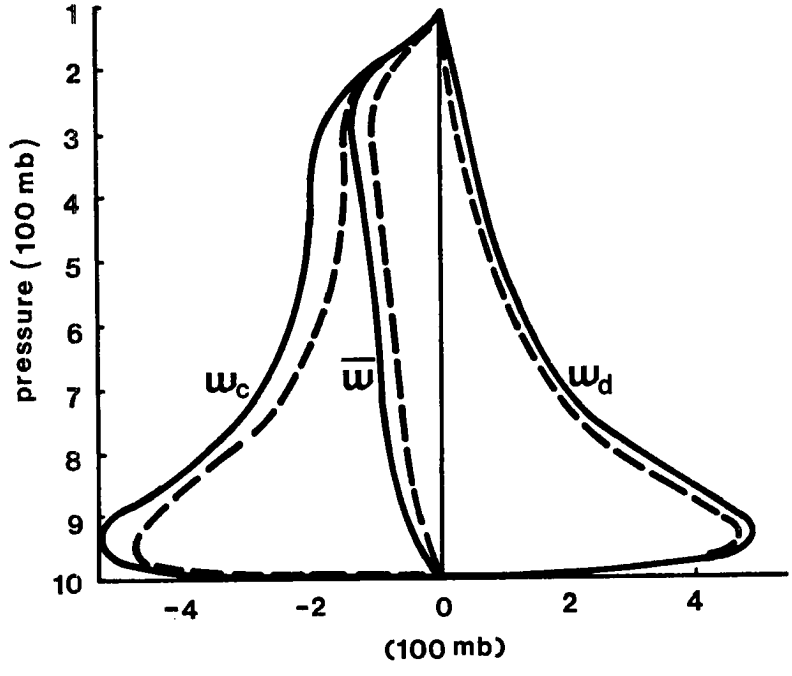

Fig. 17. Mean vertical mass flux ($\bar{\omega}$), cloud mass flux (ω_c) and downward mass flux (ω_d) for WPD4 (solid) and ATD4 (dashed) data sets when no strong downdraft is included.

tyhooon and the hurricane is again seen. These profiles are very similar to those obtained by Frank (1977c).

4.2.4 The Effect of Downdrafts on the Diagnosed Local Mass Recycling

As mentioned before, a part of the downward mass flux might be in the form of strong downdrafts which have considerably different thermodynamic aspects than those of large scale gentle subsidence. Therefore, two kinds of downdrafts other than gentle subsidence are considered, following Johnson (1976, 1980): (a) convective scale downdrafts from 350 mb (entrainment rate $\lambda = 0.05\ km^{-1}$ in Johnson's model, 1976); (b) mesoscale downdrafts from 600 mb. The difference in mixing ratio between the convective downdrafts (values are taken from Johnson, 1976) and the environment (approximated by $\bar{q}$) for the $1\text{-}5^{o}$ latitude radius average of a typhoon is shown by the dashed line in Fig. 16. The profiles for the hurricane are approximately the same as those for the typhoon. This convective downdraft is cool and dry when it reaches the surface due to re-evaporation. An increase of vertical mass recycling is expected if this convective-scale downdraft is considered because it is more moist than the environmental air.

Table 3 of Johnson's (1980) paper shows the average thermodynamic structure of mesoscale downdrafts obtained from Zipser's (1977) composite soundings. The mixing ratio for this mesoscale downdraft was reproduced from this table. The dotted line in Fig. 16 shows the mixing ratio difference between the mesoscale downdraft and the environment for the typhoon data set (WPD4). This profile shows that mesoscale downdrafts are much drier than the environment, and would thus act to reduce the amount of required vertical mass recycling for water vapor balance.

For simplicity (also due to the lack of good quantitative knowledge concerning these downdrafts), the average mixing ratio associated with all the downward motion $\bar{q}_d$ is taken to be: (a) $\bar{q}$, if $p \leq 300$ mb; (b) $(\bar{q} + q_{cd})/2$, if 300 mb $< p \leq 600$ mb; (c) $(\bar{q} + q_{cd} + q_{md})/3$, if $p >$ 600 mb; where subscripts cd and md represent cloud downdraft and mesoscale downdraft respectively. The vertical mass recycling at each level is thus given by

$$(\omega_r) = - Q_r g/(\bar{q}_s - \bar{q}_d) \qquad [25]$$

and cloud and downward mass fluxes are determined by Eqs. 23 and 24. These results are shown in Fig. 18 where the low level vertical mass flux is slightly reduced. It must be remembered that the profiles shown in Fig. 18 will certainly vary from reality due to the assumptions involved in this simple model. However, these profiles are still physically reasonable and show consistency for both ocean basins.

As mentioned before, the ratio of the mean vertical motion to the calculated local recycling has to match the ratio of the assumed condensation to rain produced by the mean vertical motion and the condensation to rain produced by the local recycling. Figure 19a depicts the assumed profiles of condensation to rain for the three quantities of R_m, R_r and R at each level. Note that these profiles resemble those of $\bar{\omega}$, ω_r and ω_c quite well. It should be noted that the calculated local recycling profile is very sensitive to the assumed vertical distribution of R_r (or R). If a larger R_r is assumed at lower levels, the magnitude of ω_r is reduced substantially at all the higher levels. For comparison purposes, the ratios of the assumed R_m to R and of the $\bar{\omega}$ to the calculated ω_c are shown in Fig. 19b. These two profiles are almost identical at middle to lower levels. At upper

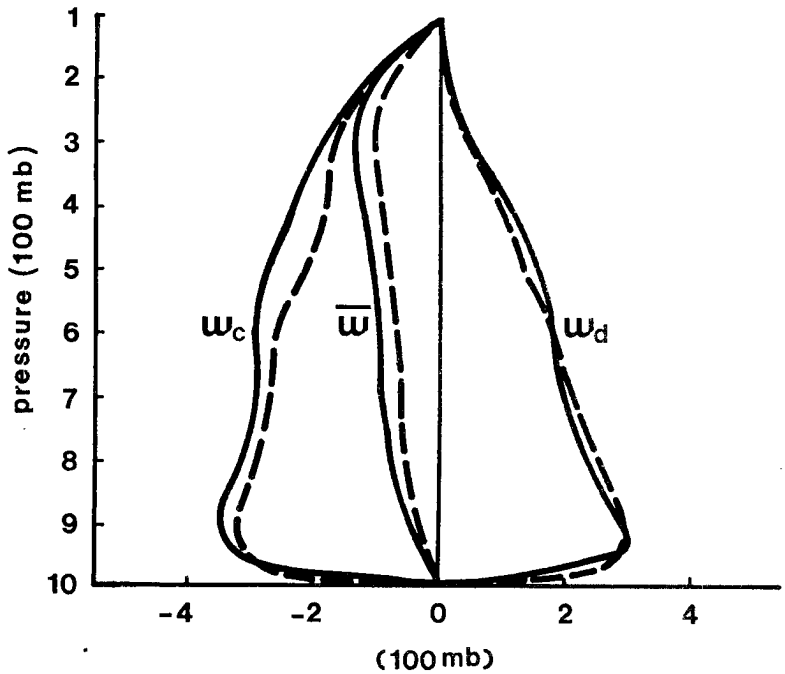

Fig. 18. Mean vertical mass flux ($\bar{\omega}$), cloud mass flux (ω_c) and downward mass flux (ω_d) for WPD4 (solid) and ATD4 (dashed) data sets when both kinds of downdrafts are included.

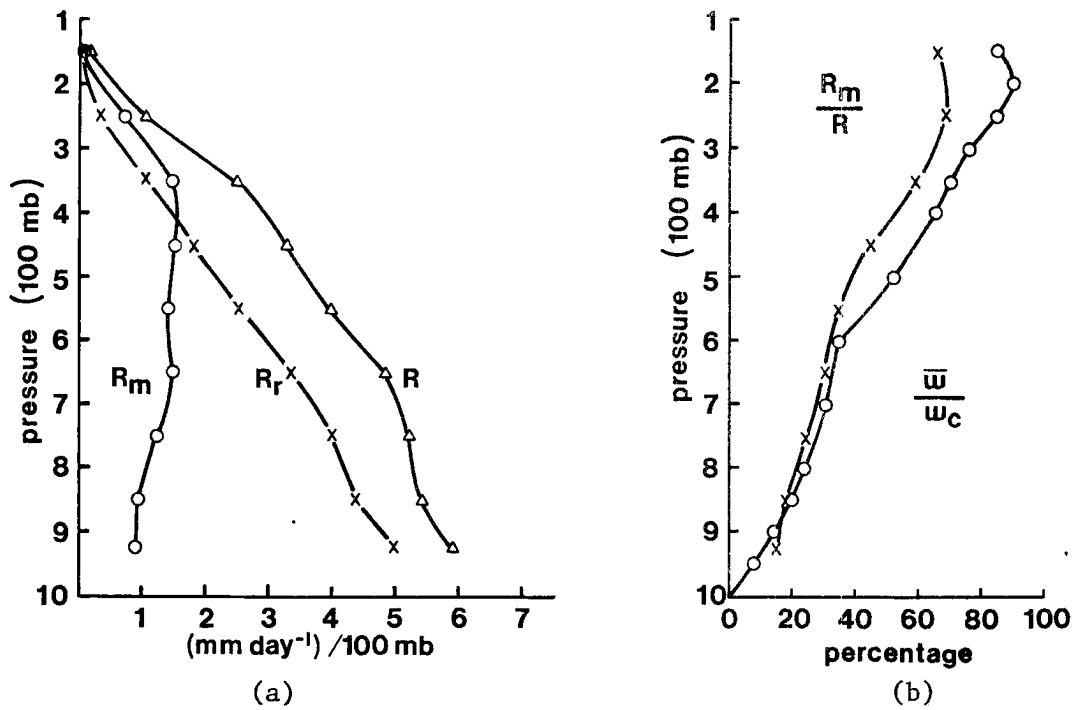

Fig. 19. (a) Condensation to rain for every 100 mb layer due to mean vertical mass flux (R_m), local mass recycling (R_r) and the total upward mass flux (R). (b) Ratios of R_m to R compared to that of mean vertical mass flux ($\bar{\omega}$) to the total upward mass flux (ω_c).

levels, the difference is a little larger. This is because the condensation magnitudes are much smaller at upper levels and a small calculation error can cause larger percentage differences. The agreement of these profiles provides good support to this mass recycling model.

4.3 Tangential Momentum Associated With Upward and Downward Motions

Besides upward and downward mass fluxes, the tangential momentum associated with cloud updrafts and/or downdrafts is still required in order to fully evaluate Eq. 15 or Eq. 18. It is likely that the cloud momentum should vary as the ascending air parcel entrains and/or mixes with the environmental air. Since deep cumulus convection has a very short parcel time scale, this vertical variation of cloud momentum should be negligibly small (Schneider and Lindzen, 1976; Stevens et al., 1977). Indeed, the diagnosed cloud momentum of Shapiro and Stevens (1980) appears to be fairly constant with height with a magnitude close to the environmental momentum at cloud base height (950 mb). The cloud momentum values assumed for this study are shown by the solid lines in Figs. 20a and 20b. These cloud momentum values are assumed to vary in the vertical as the ascending air entrains environmental air. A small constant mixing rate (both entrainment and detrainment) between clouds and the environment is also used.

In the diagnosis of vertical mass recycling, the effects of cloud downdrafts and mesoscale downdrafts are also considered as those in the cumulus parameterization scheme (Eq. 18). The vertical profiles of momentum associated with these two kinds of downdrafts are shown by the dotted lines in Fig. 20. The net entrainment and mixing effects again are considered to allow these downdrafts to exhibit different momentum

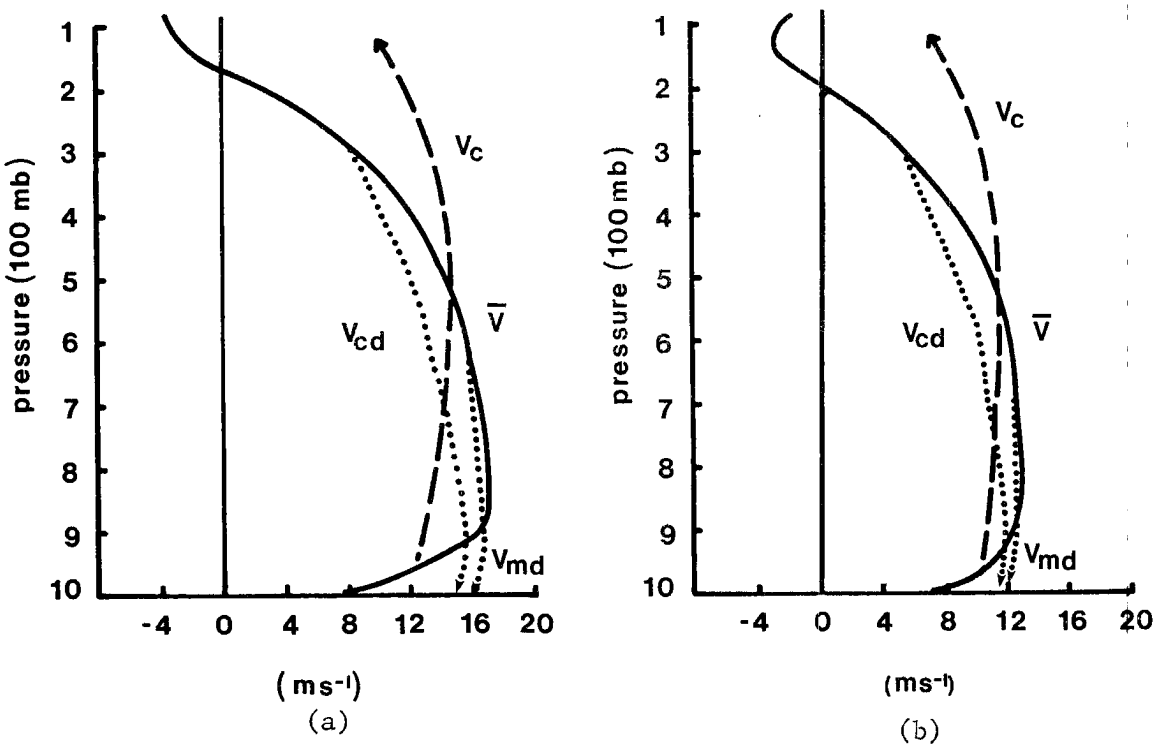

Fig. 20. Mean tangential wind profile ([$\bar{v}$]) and tangential momentum associated with cloud updrafts (V_c), cloud downdrafts (V_{cd}) and meso-scale downdrafts (V_{md}) for (a) typhoon (WPD4) and (b) hurricane (ATD4) data sets.

characteristics as they descend. As discussed before, the momentum associated with the broadscale subsidence is considered to be the same as the grid-box average momentum (Eq. 13). Such an assumption is somewhat violated especially at the lower levels where deep and shallow convective clouds cover a significant percentage of the total area.

Although convective clouds are considered to transport environmental momentum up and down, it is unlikely that such assumed momentum profiles can be observed locally in individual cases. Complications arise due to the usually observed mesoscale high pressure associated with convective cells (Zipser, 1977). Such convective-induced pressure gradients might cause a substantial alteration of the momentum fields locally. However, it is possible that such assumed

momentum profiles can be obtained by compositing many observed momentum profiles associated with many convective systems. In this composite situation, such pressure gradient forces will probably average to zero.

4.4 Results and Discussions

The dashed lines in Fig. 21 show the model-diagnosed cumulus friction without strong downdrafts (Eq. 15). The solid lines represent the residual cumulus friction. Remarkable consistency was found between the model diagnosis and the calculated residuals for both the typhoon and the hurricane. The differences between these two profiles for both oceans are within the limits of calculation error except at 700 mb for the typhoon case where the difference appears too large to be accounted for by computation noise. This may be due to the fact that horizontal eddy effects were neglected in the residual calculations (see Fig. 4). These results are more consistent than those (momentum fields) obtained by Shapiro and Stevens (1980). This is probably because an evaluation of the pressure gradient force was required in their calculations but not in this analysis. This may be especially relevant at the upper levels where pressure gradient measurements are most unreliable.

The use of $D_n = 1/3$ in Eq. 18 for both cloud downdraft and mesoscale downdraft only changes the low level results slightly, as shown by the dotted lines in Fig. 21. Thus, although strong downdrafts have to be considered in diagnosing the correct vertical mass recycling, such strong downdrafts can be largely neglected in cumulus momentum parameterization schemes. However, such a conclusion is somewhat dependent on the middle to low level vertical wind shear which is very small in these cases. It is possible that strong downdrafts can play a much more important role if the middle to low level wind shear is large.

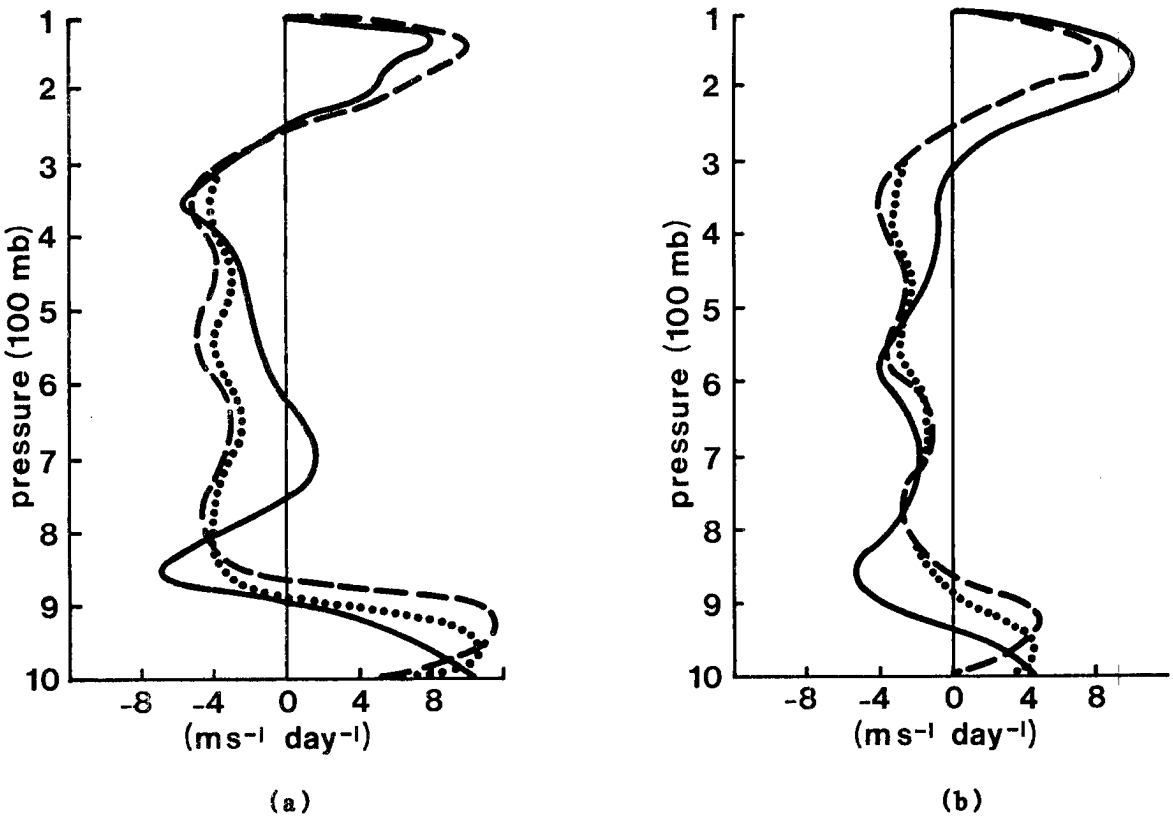

Fig. 21. Model diagnosed cumulus friction with (dotted) and without (dashed) both kinds of downdrafts compared to the residual cumulus friction (solid) for (a) typhoon (WPD4) and (b) hurricane (ATD4) data sets.

Although only a simple single cloud model is used to parameterize cumulus friction, the model-diagnosed results agree reasonably well with the calculated residuals in both pattern and magnitude. This is as good as one might expect given the limitations of both the observational data and the theoretical model assumptions. This simple scheme (Eq. 15) has also been used by Stevens et al. (1977) and Fingerhut (1982) in numerical model studies which yielded realistic results.

Note that all the discussions here are on the net effect of cumulus convection on the large-scale momentum fields. This net effect appears to be not strongly dependent on the detailed internal dynamics of the

convective systems (also discussed by Cho et al., 1979; Shapiro and Stevens, 1980). However, the cloud internal dynamics must be taken into account should a single convective cell or mesoscale system be considered.

Shapiro and Stevens (1980) also emphasized the importance of the correct determination of the cloud mass flux. However, although the cloud mass flux diagnosed in section 4.2 may not be exact, realistic results were still obtained. It is probable that this parameterization scheme is more sensitive to cloud momentum than to cloud mass flux. More observational studies of a spectrum of cloud momentums are needed to confirm fully these model results. Aside from all these assumptions and complications, we were nevertheless gratified to learn that there was general consistency between the calculated residuals and the model diagnosed results. This provides a good justification to the hypothesis that the calculated residual at inner $1-5^{o}$ latitude radii of a tropical cyclone system is a realistic estimate of cumulus friction.

5. THE ROLE OF CUMULUS MOMENTUM TRANSPORTS

McBride and Zehr (1981) found that the most distinct difference between developing and non-developing cloud clusters is the environmental vertical wind shear: the developing system is embedded in an environment with much larger vertical wind shear. A zero vertical wind shear line extends across the center of the developing system. As the system intensifies from a cloud cluster to a mature tropical storm, the vertical wind shear also increases over a very large radial domain. This increase in vertical wind shear is largely due to the increase of mid-low level cyclonic wind at inner radii and to the increase of upper level anticyclone wind at outer radii (Fig. 22).

As have been discussed by Silva Dias and Schubert (1979), and Schubert et al. (1980), geostrophic or cyclostrophic adjustment on the cyclone scale in the tropics is primarily an adjustment of the mass field to the wind field. Thus, for genesis and intensification to occur a tropical system must form an anticyclonic vertical wind shear around its center (1-5^{o} latitude radius region or even further outward) to sustain an upper level warm core. This upper level warm core is primarily attributed to the release of latent heat (in form of subsidence warming) of cumulus convection. The understanding of how this vertical wind shear can increase during the evolution of the system becomes fundamentally important to the tropical cyclone genesis and intensification problem.

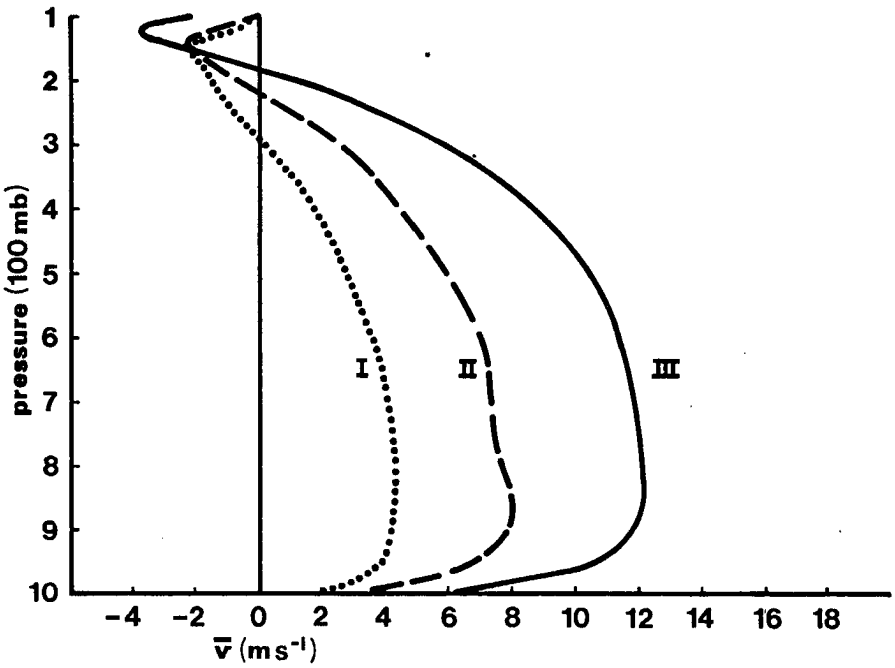

(a)

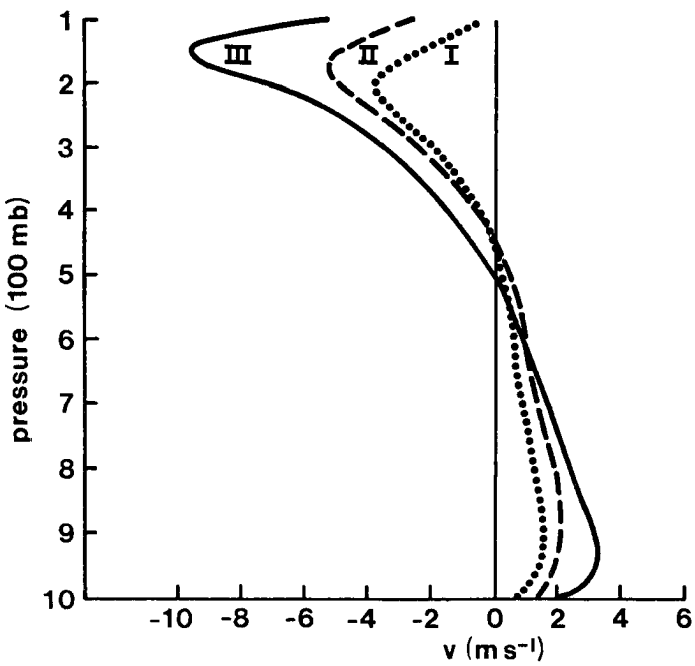

(b)

Fig. 22. Vertical profiles of the mean tangential wind at (a) 1-5° latitude radial belt and (b) 10° latitude radius for cloud cluster (I), tropical depression or storm (II), and mature typhoon or hurricane (III).

5.1 Total Convective Effect (TCE)

The previous discussions suggest that the net effect of the cumulus-induced pressure gradient is not important when averaged over a large area (or around the system center at any radius). It is still necessary, however, to examine the influences of all the vertical motion on the tangential momentum field before the down-gradient or up-gradient nature of the cumulus convection processes can be determined. In section 4.1, the total convective effect (TCE) is decomposed into the mean $(-\partial(\overline{[\omega][v]})/\partial p)$ and eddy $(-\partial\overline{[\omega'v']}/\partial p)$ vertical transports (Eq. 14). The mean vertical transport can be directly calculated and the eddy convective transport is approximated by the calculated residual in the TCE calculation.

The TCE profiles for the 16 composited tropical cyclone data sets within the $1-5^{o}$ latitude radius region around the system center are depicted in Figs. 23-30. These profiles show systematic variations similar to those of the residual cumulus friction, because the mean convective transport has the same pattern (negative acceleration at lower levels and positive acceleration at upper levels) for all the data sets. The triangle on each curve shows the level of maximum cyclonic wind. It is here where a pronounced negative acceleration influence (which acts to spin down the cyclonic momentum) is found for every data set. For most of the data sets this level is around 950-800 mb where the strongest convergence is typically found. The exceptions are the non-developing cluster data sets (WPN1, ATN1) which have their maximum cyclonic wind at a higher level (600 mb and 500 mb). A pronounced positive value (minimum negative for ATN1) is found near 150-300 mb where the maximum divergent layer (or deep cloud detrainment layer)

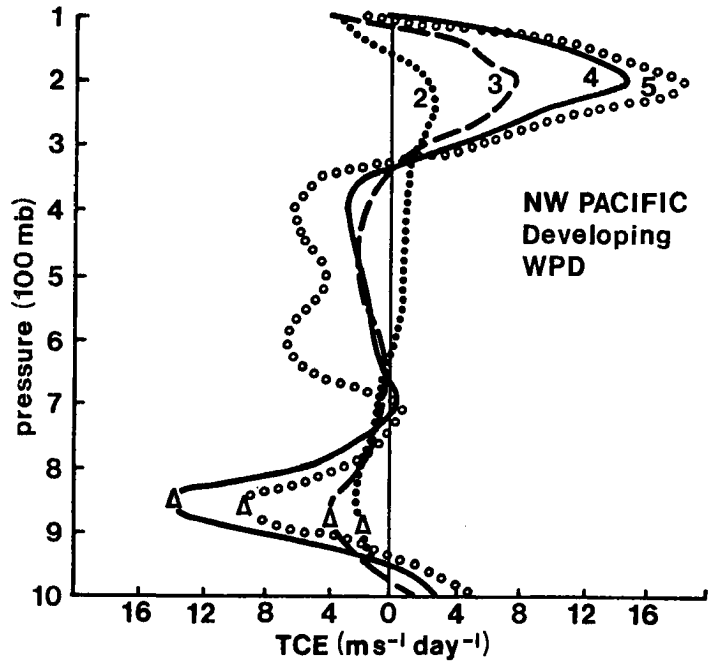

Fig. 23. 1-5° latitude radial and azimuthal averages of total convective effect (TCE) for the northwest Pacific (WP) developing tropical cyclone systems: a) WPD2 (cloud cluster), b) WPD3 (intensifying tropical storm), c) WPD4 (mature typhoon) and d) WPD5 (supertyphoon). The triangle shows the level of maximum cyclonic wind.

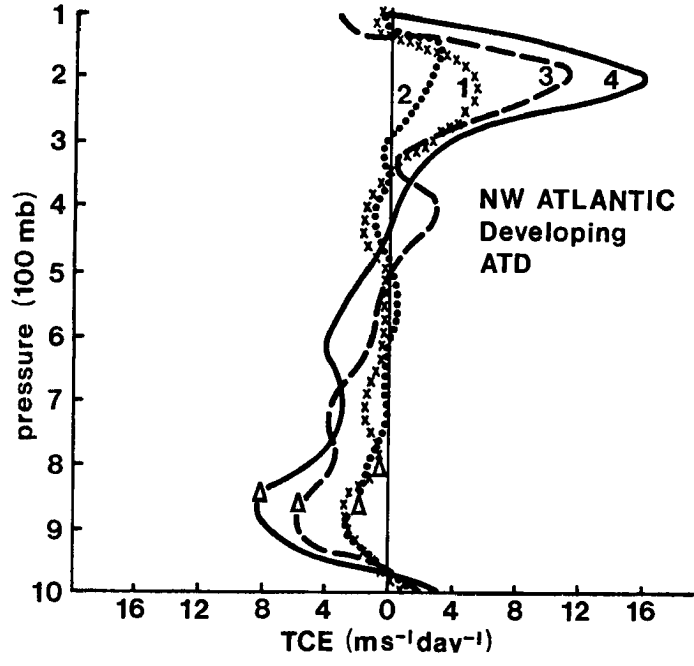

Fig. 24. 1-5° latitude radial and azimuthal averages of total convective effect (TCE) for the northwest Atlantic developing tropical cyclone systems: a) ATD1 (cloud cluster), b) ATD2 (tropical depression), c) ATD3 (intensifying tropical storm) and d) ATD4 (mature hurricane). The triangle shows the level of maximum cyclonic wind.

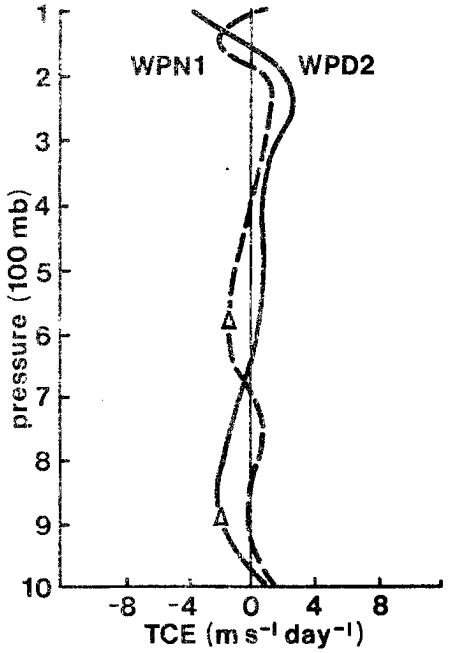

Fig. 25. The same as Fig. 23 but for developing (WPD2) and non-developing (WPN1) cloud clusters in the northwest Pacific.

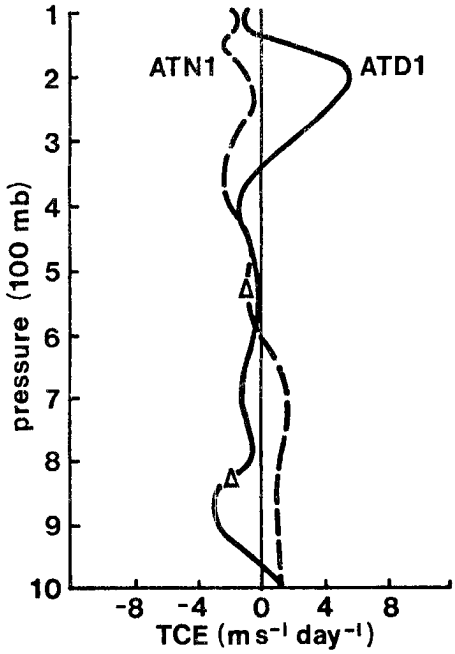

Fig. 26. The same as Fig. 23 but for developing (ATD1) and non-developing (ATN1) cloud clusters in the northwest Atlantic.

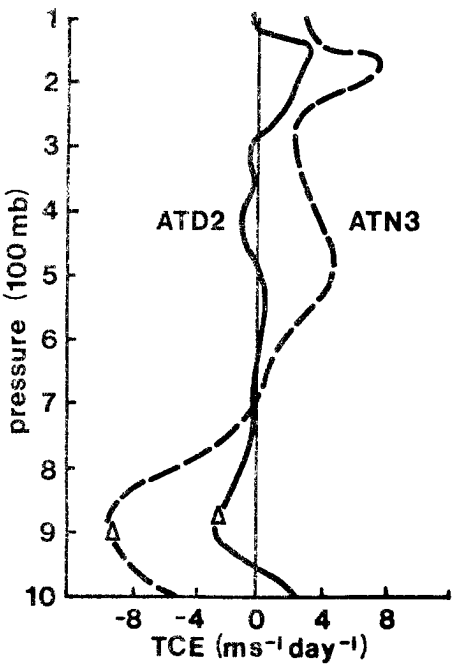

Fig. 27. The same as Fig. 23 but for developing (ATD2) and non-developing (ATN3) tropical depressions in the northwest Atlantic.

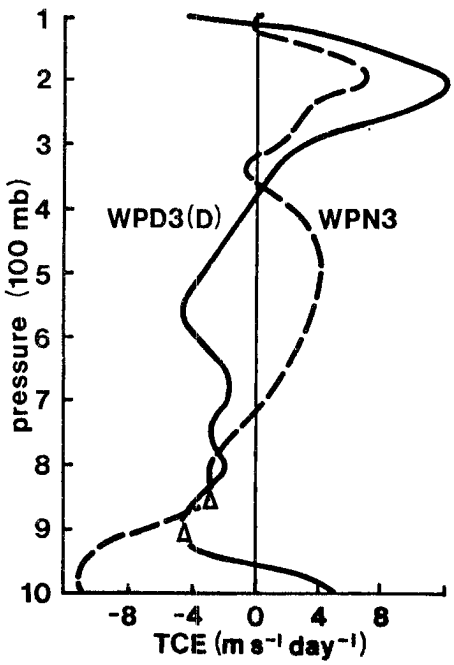

Fig. 28. The same as Fig. 23 but for deepening (WPD3(D)) and non-developing (WPN3) tropical storms in the northwest Pacific.

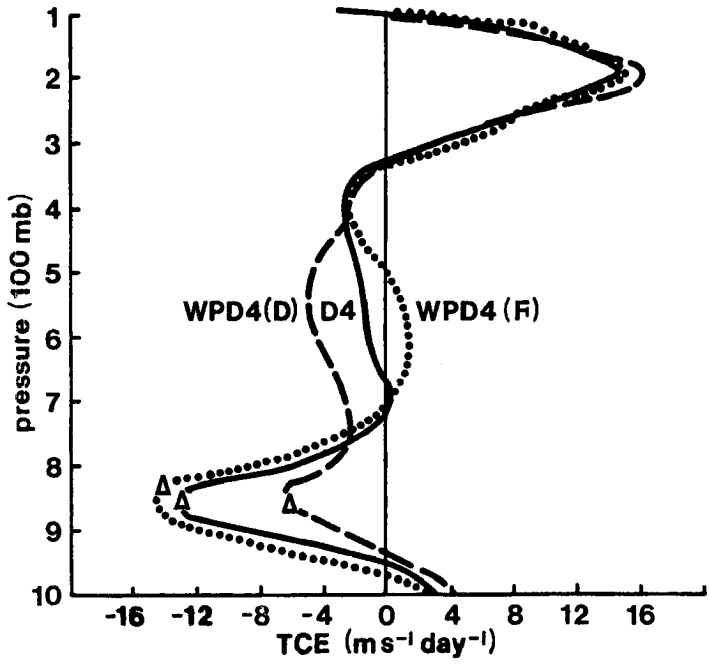

Fig. 29. 1-5° latitude radial and azimuthal averages of total convective effect (TCE) for mature (WPD4), deepening (WPD4(D)) and filling (WPD4(F)) typhoons in the northwest Pacific. The triangle shows the level of maximum cyclonic wind.

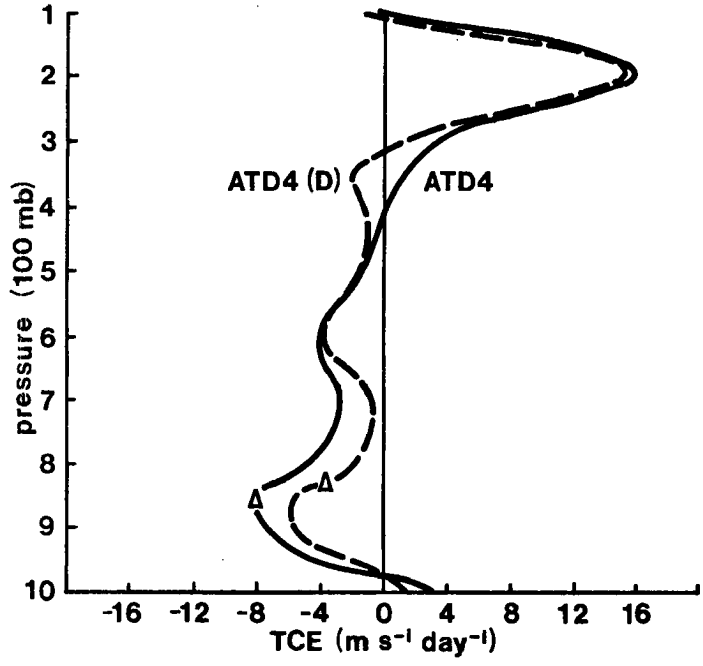

Fig. 30. 1-5° latitude radial and azimuthal averages of total convective effect (TCE) for mature (ATD4) and deepening (ATD4(D)) hurricanes in the northwest Atlantic. The triangle shows the level of maximum cyclonic wind.

exists.

These consistent results lead to the conclusion that convective clouds act in a down-gradient mixing sense to rearrange horizontal momentum vertically in the following way:

a) Low level cyclonic momentum is brought up by (deep) cloud updrafts and detrained in the upper levels. This results in a pronounced positive TCE in the upper layers and a negative TCE in lower layers. Such processes act to decrease both the upper level anticyclonic and the low level cyclonic winds.

b) The tendency of TCE (or cuF_θ) to be positive near the surface is likely due to downward motions from higher layers or to vertical turbulent mixing processes at lower layers.

c) Pure vertical mixing processes will cause a momentum loss at the level of maximum cyclonic wind as is observed for all the 16 data sets.

d) Although up-gradient momentum transport, possibly caused by small-scale dynamic effect, might occur in individual convective system and act to increase the local vertical wind shear (as observed and suggested for individual intense systems by Betts et al. 1976; Moncrieff and Miller, 1976), the net small-scale dynamic effect of all convective systems on the large scale momentum fields is not that important and the down-gradient mixing process appears to be dominant.

5.2 Mean and Eddy Vertical Transports

The mean ($-\partial\overline{[\omega][v]}/\partial p$) and eddy ($-\partial\overline{[\omega'v']}/\partial p$ or cuF_θ) vertical transports of tangential momentum appear to exhibit the same pattern for all the developing cases, with the stronger systems having larger magnitudes (refer to Figs. 5- 6 and Figs. 23-24). To compare these two transport processes, an average of all the developing systems (WPD2, WPD3, WPD4(D), ATD1, ATD2, ATD3 and ATD4(D)) has been taken. Results are shown in Fig. 31. The total convective effect (or the sum of these two processes) is also shown. Note that all these data sets (which are averaged together) are independent. This figure shows that cumulus friction is always comparable to (or even greater than) the mean

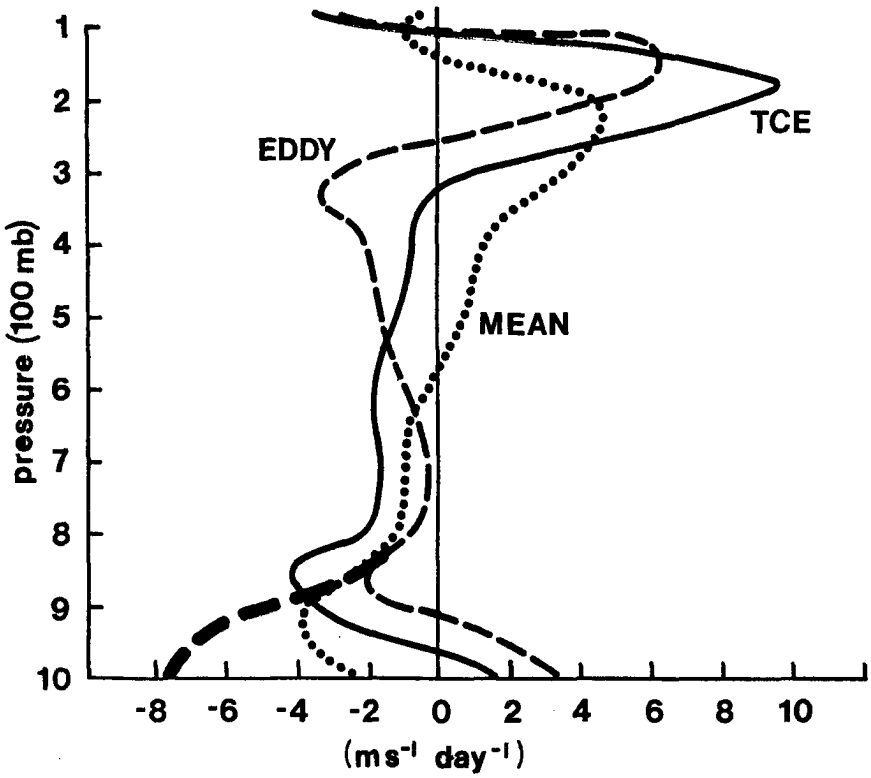

Fig. 31. Averaged vertical profiles of total convective effect or TCE (solid), and that part of the TCE accomplished by the mean vertical motion or $-(\partial[\omega][v]/\partial p)$ (dashed) and that part accomplished by the eddy process or $cuF_{o\theta}$ (dotted) for all the developing data sets in the region 1-5° latitude radius around the system center. The heavy dashed curve is when the surface friction is added to the cumulus friction.

vertical transport in magnitude and its pattern is quite similar to the TCE. These results indicate that cumulus friction is an important physical process and ought to be taken into account in numerical model simulations of tropical cyclones.

The pattern of this cumulus friction agrees well to that of the apparent vorticity source calculated by Williams and Gray (1973) and Reed and Johnson (1974). Their results show a positive momentum or vorticity source at the upper outflow layer and a negative source at middle and lower layers (surface friction was not taken out in their calculation). When the surface friction is added to the present cumulus

friction, results show (heavy dashed curve in Fig. 31) only a stronger low level negative acceleration.

Alternatively, the symmetric equation of tangential momentum can be written in an advection form as:

$$\frac{\partial[\bar{v}]}{\partial t} = \overline{-[u]\,[\zeta_a]} - \overline{[\omega]\,\frac{[\partial v]}{\partial p}} + \overline{[cu\,F_\theta]} + \overline{[sF_\theta]} \qquad [26]$$

where $\zeta_a = (\frac{\partial \bar{v}}{\partial r} + \frac{\bar{v}}{r}) + f$ is the absolute vorticity. The term $\frac{\bar{v}}{r}\frac{\partial \bar{v}}{\partial \theta}$ has been neglected in Eq. 26 because it is always much smaller than other terms. The first term on the right hand side represents the horizontal advection; and the second and the third terms are the vertical advection (VA) and vertical eddy transport (or cuF_θ) respectively. Vertical profiles of the last two terms are shown in Fig. 32. Note that the sum of these two terms do not vertically integrate to zero. Equation 26 provides a simpler way to see how the vertical motion processes can act to produce a negative tangential acceleration through a deep layer - up to 300 to 350 mb. A similar approach has been previously taken by Gray (1967) to study momentum changes within the eye-wall regions of hurricanes.

5.3 Environmental Wind Fields and Cumulus Friction

Because cumulus convection is primarily a down-gradient mixing process, the total convective effect must correspond to the environmental vertical wind shear and the intensity of the convection. Since the mean convective effect has almost the same vertical pattern for all the data sets, the change in the vertical pattern of TCE appears to be largely determined by the change in the cumulus friction profile. Furthermore, if the vertical mass recycling is assumed to have the same pattern as that shown in Fig. 18 for all the data sets, we can limit our

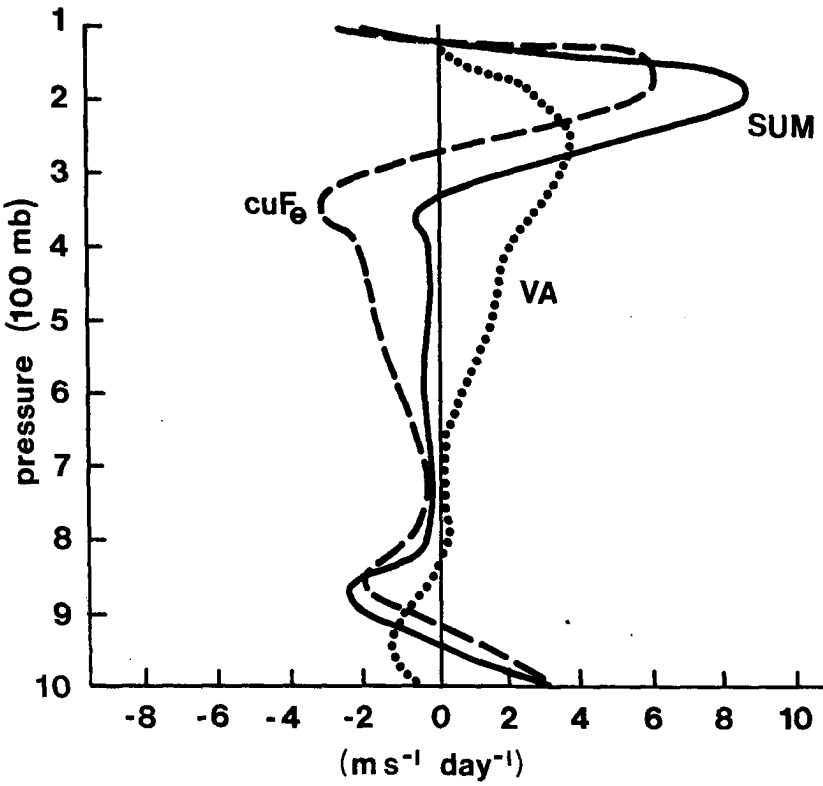

Fig. 32. Averaged vertical profiles of cumulus friction (dashed), vertical advection (VA) tangential momentum by mean vertical motion (dotted) and the sum of these two (solid) for all the developing data sets in the region 1-5° latitude radius around the system center.

discussion to the relationship between the cumulus friction profile and the mean vertical motion and tangential wind fields. To study the dependence of the cumulus friction on the environmental wind fields data sets are grouped into 3 different intensity stages. Each stage includes both developing (D) and non-developing/steady (N) cases as shown in Table 6. Note that WPD4 and ATD4 (or III-N category) are not deepening but have a steady or filling tendency trend.

TABLE 6

The data sets which are grouped into different categories.

	Developing (D)	Non-developing/steady (N)
(I) Initial Stage	(I-D) WPD2,ATD1	(I-N) WPN1,ATN1
(II) Intermediate Stage	(II-D) WPD3,ATD2,ATD3	(II-N) WPN3,ATN3
(III) Mature Stage	(III-D) WPD4(D),ATD4(D)	(III-N) WPD4, ATD4

Figures 33 and 34 illustrate the averaged vertical profiles (for I, II and III stages) of cumulus friction, tangential wind, and mean vertical motion for the developing (D) and non-developing/filling (N) cases. The profiles of each of these three parameters share similar vertical patterns for the D and N cases, though the magnitudes are different. These cumulus friction profiles are similar to those diagnosed by Hack and Schubert (1980) except at lower levels where our developing cases have a smaller amplitude.

For the developing cases, the cumulus friction does not change its vertical pattern from initial to mature stage. Its amplitude however increases substantially with intensity (Fig. 35a). This is quite reasonable because the mean vertical motion and vertical tangential wind profiles are not much different among developing systems (Figs. 35b, 35c), and thus the cumulus friction patterns do not vary much. The increasing magnitude of cumulus friction is just a result of the increase in the vertical wind shear (see Eq. 15).

It is more complicated to discuss the non-developing/steady cases since none of the individual composite profiles resembles the average profiles of Fig. 33. Note that the intensity classifications (I-N,

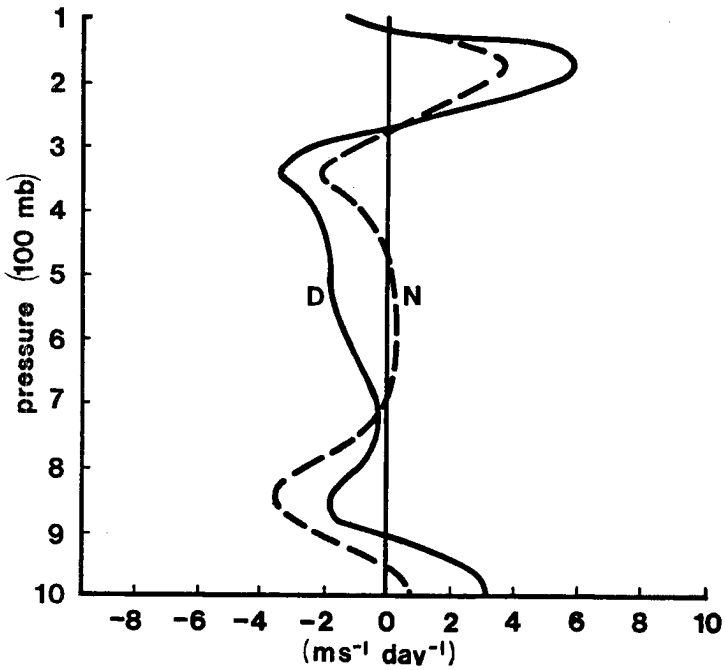

Fig. 33. Averaged vertical profiles of cumulus friction (cuF_θ) for all developing (D) and non-developing/steady (N) cases in the region 1-5° latitude radius around the system center.

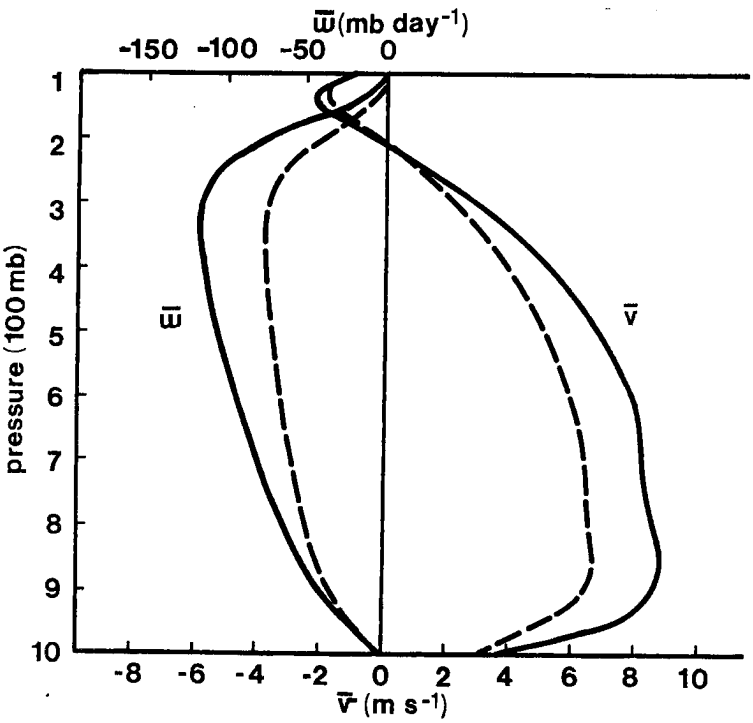

Fig. 34. Averaged vertical profiles of mean vertical motion and tangential wind for developing (solid) and non-developing (dashed) data sets in the region 1-5° latitude radius around the system center.

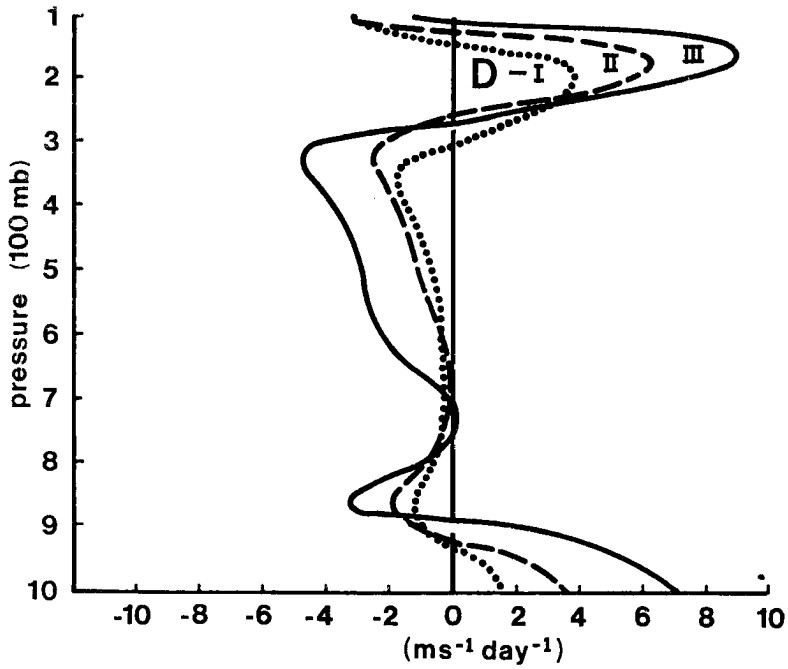

(a)

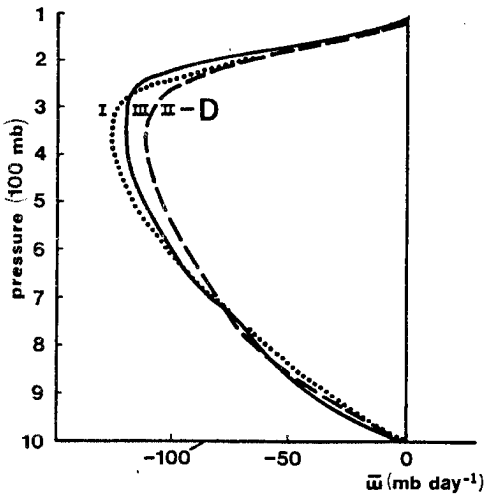

(b)

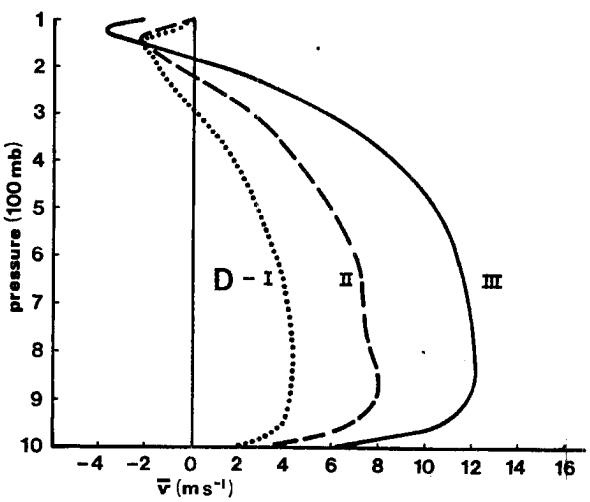

(c)

Fig. 35. 1-5° latitude radial and azimuthal averages of (a) cumulus friction, (b) mean vertical motion and (c) tangential wind for the developing tropical cyclone systems of cloud cluster (I), tropical depression or storm (II) and mature typhoon or hurricane (III) stages.

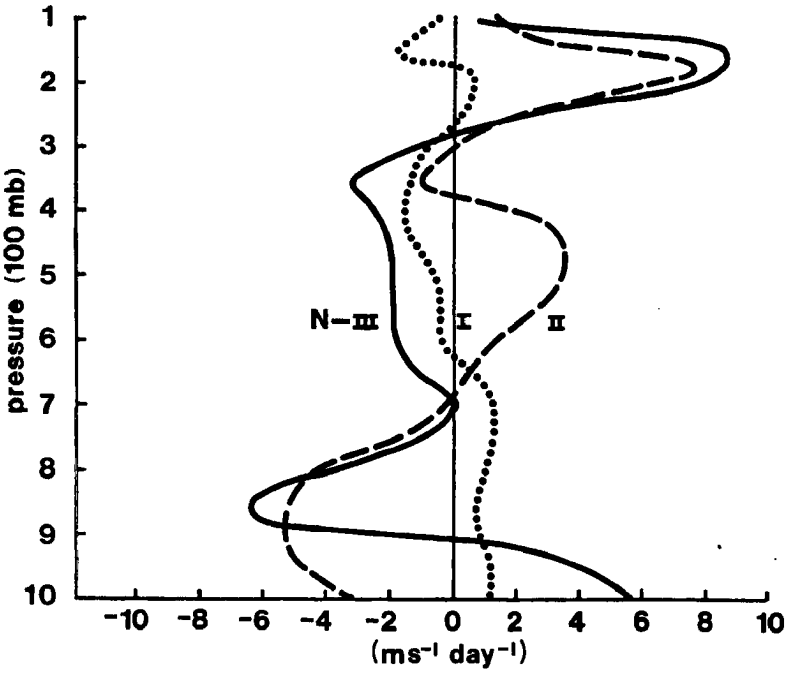

(a)

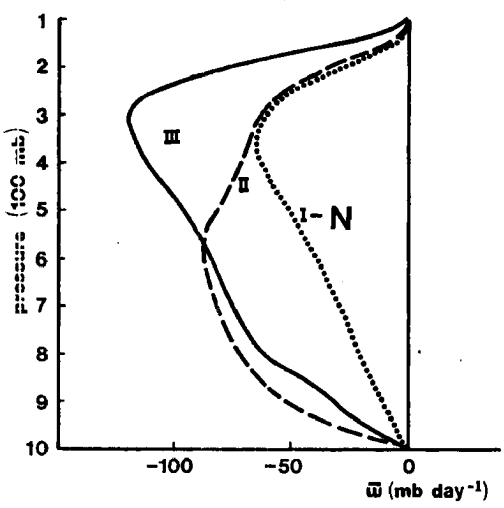

(b)

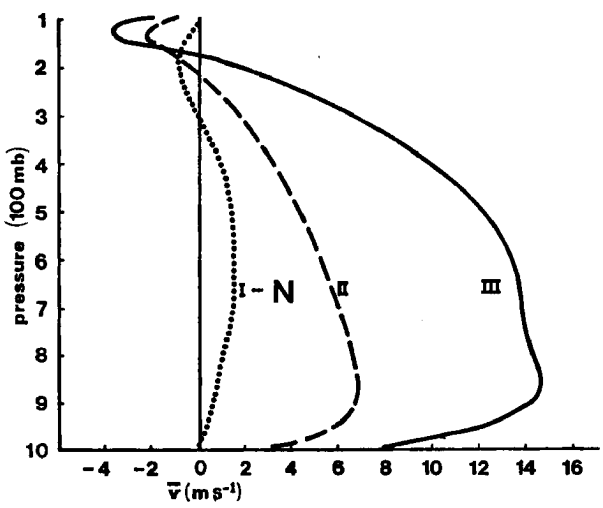

(c)

Fig. 36. 1-5° latitude radial and azimuthal averages of (a) cumulus friction, (b) mean vertical motion and (c) tangential wind for the non-developing tropical cyclone systems of cloud cluster (I), tropical depression or storm (II), and mature typhoon or hurricane (III) stages.

II-N and III-N) are not a progressive increase as with the developing cases. The mean vertical motion and vertical tangential wind profiles are shown in Figs. 36b,c. Obviously, the patterns of these profiles differ from one another and also from those of the developing cases. This results in the different profiles of cumulus friction. For the initial stage, not much difference exists in the mean vertical motion patterns (except the magnitude) between the I-N and I-D cases; however, the tangential wind profiles do show important differences. The I-D case (also II-D and III-D) has the level of maximum tangential wind at about 850 mb and little vertical wind shear from 600-900 mb. Contrary to the I-D case, the tangential wind of the I-N case has a maximum at about 500-700 mb and decreases to zero (or slightly negative) at the surface. The positive cumulus friction for the I-N case from 700 mb down to the surface is probably a result of this wind shear in the middle to low levels and the effect of downdrafts or downward mass flux.

For the intermediate stage, a slightly larger 600-900 mb vertical wind shear is found for the II-N compared with the II-D case. The most appreciable difference is in the mean vertical motion. Since the vertical mass recycling strongly decreases with height, the decrease of the mean vertical motion at 400-600 mb for the II-N case implies a secondary divergent layer other than the major upper outflow layer. This secondary divergent layer and the vertical wind shear yield a positive value of cumulus friction between 400-650 mb for the II-N case. For the III-N case the patterns of tangential wind, vertical motion, and cumulus friction are quite similar to those of the developing case (III-D). But the magnitude of the cumulus friction is larger for the III-N case. This is a result of the greater vertical wind shear of this

system.

The above discussions again support the contention that cumulus convection is primarily a down-gradient mixing process, and hence the cumulus friction profile has to correspond to the environmental flow features. Therefore, in a numerical model, cumulus friction ought to be determined (or parameterized) according to the simultaneously corresponding flow features and surface energy fluxes (or evaporation) manifested through the vertical mass recycling (as discussed in Chapter 4).

5.4 The Effects of Cumulus Convection on the Upper Outflow Layer

The net effect of cumulus convection on the upper outflow layer is to decrease the anticyclonic winds. This is equivalent to an increase in absolute angular momentum of the outward moving air parcels. An air parcel has to conserve its absolute angular momentum along its trajectory unless acted upon by a torque. However, trajectory analyses for hurricane (ATD4) and typhoon (WPD4) systems show an increase of absolute angular momentum associated with outflowing air parcels.

The trajectory analysis on the 150 mb isobaric surface, the level of maximum concentrated outflow, has been carefully made. The composite storm is assumed to be in a steady state and moving with constant direction and speed. Streamline patterns are obtained at two different 12 hour times, and trajectories constructed (see Saucier, 1955, p. 313 for a description of the procedures used). Figure 37 depicts an example of how these trajectories are determined. Such an analysis was performed for the typhoon (WPD4) and hurricane (ATD4) data sets. Figure 38 shows the trajectories and the constant absolute angular momentum contours at 150 mb for the mean typhoon and mean hurricane. Absolute

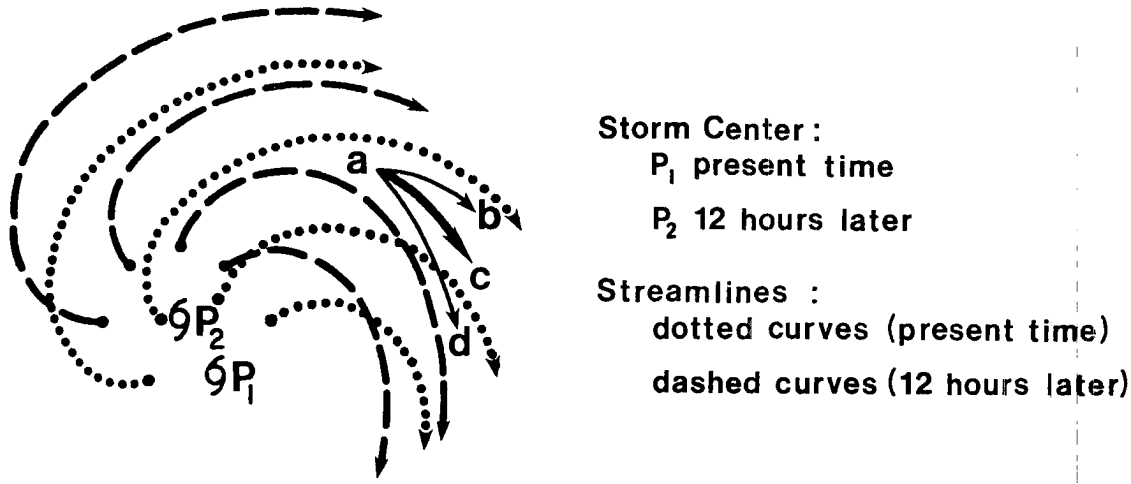

Fig. 37. Schematic diagram showing how the outflow trajectory was constructed. Curves ab and ad are the paths that an air parcel will travel in 12 hours from point a if it follows the stream lines of the present time (ab) and of 12 hours later (ad), respectively. The length of ab and ad is determined by the wind speed. The curve ac is the trajectory that an air parcel will travel from point a in this 12 hour period with respect to the moving storm center P.

angular momentum, M_a, is defined as:

$$M_a = 1/2\ f_o r^2 + rv$$

where f_o is the Coriolis parameter at the system center. These figures show that the absolute angular momentum of an air parcel generally increases as they move outward from the storm center.

For an individual air parcel, however, there may still be a pressure gradient force acting upon it. This will also cause a change of absolute angular momentum along the trajectory. But when all the trajectories crossing a certain radius are considered the net tangential pressure gradient force is zero and the absolute angular momentum will still increase along the trajectory, especially at inner regions. This suggests the importance of the TCE in modifying the radial circulation at the inner region ($r < 5^o$ latitude) around the system center. It is also worthwhile to notice that the greatest crossing angle occurs inside

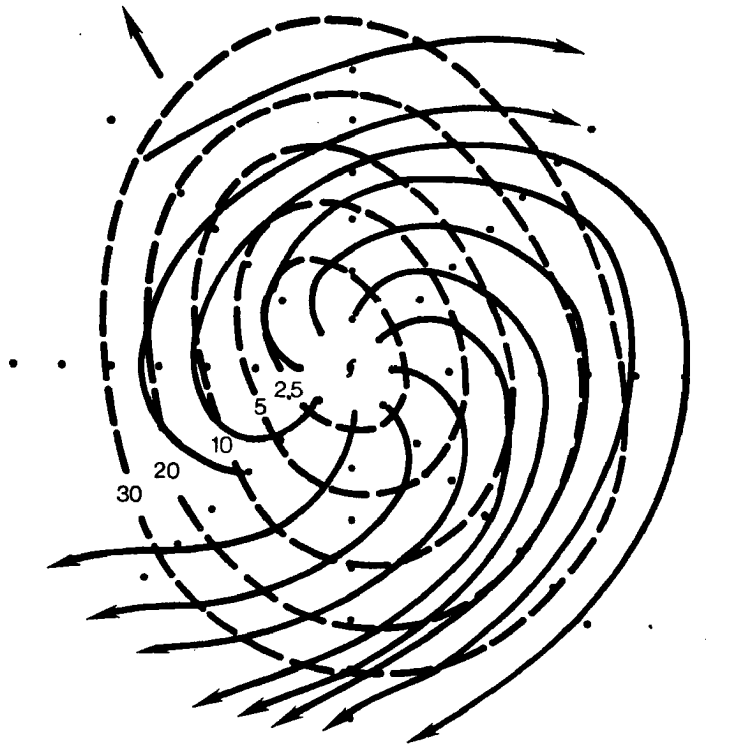

(a)

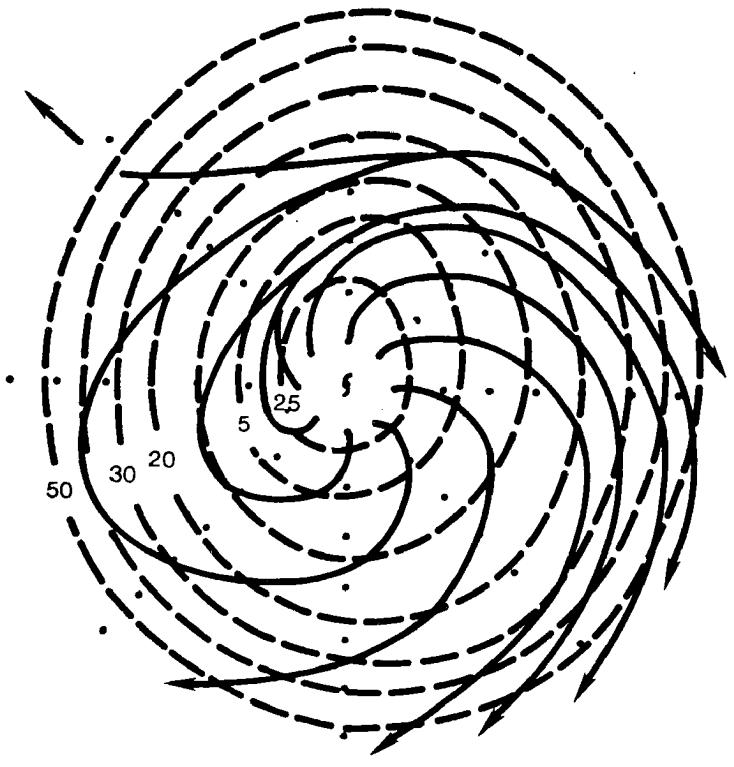

(b)

Fig. 38. Trajectories (solid) and absolute angular momentum (dashed) in 10^6 $m^2 s^{-1}$ at 150 mb isobaric surface for (a) WPD4 (typhoon) and (b) ATD4 (hurricane) data sets. Arrow points the direction of the storm motion.

about 5^{o} latitude radius and to the south of the storm center.

5.5 Discussion

It has been generally accepted that the low level convergence in a tropical cyclone system is primarily due to surface frictional effects. However, the composite data show that for a developing storm the inflow can extend up to 300 mb. This deep inflow layer is probably an important factor in differentiating a developing system from a non-developing one. Figures 39 and 40 show a cross-section of the azimuthally-averaged radial wind for developing vs. non-developing systems in both ocean basins. It is obvious that the developing systems have a much deeper inflow, especially within the inner $2-4^{o}$ radius region. Note, however, that the non-developing systems have a more concentrated low level inflow.

It is possible that this radial circulation (deep inflow layer) is affected by the cumulus convection, as has been discussed in the last section. Eliassen (1951) showed that a radial circulation has to respond to an angular momentum or heat source in a stable circular vortex. The pattern of this radial circulation is largely determined by the inertial stability of the vortex flow (see also Schubert and Hack, 1981). Generally speaking, this radial circulation can be considered as a secondary circulation to wipe out the imbalance between the large scale pressure and wind fields. The present results again show similar patterns between the radial wind and the TCE profiles (refer to Figs. 27, 28, 39 and 40). Therefore, the mutual interaction between the small scale cumulus convection and the large scale radial (and tangential) flow features during tropical cyclone development appears to be very important. However, the exact relationship between the radial wind and

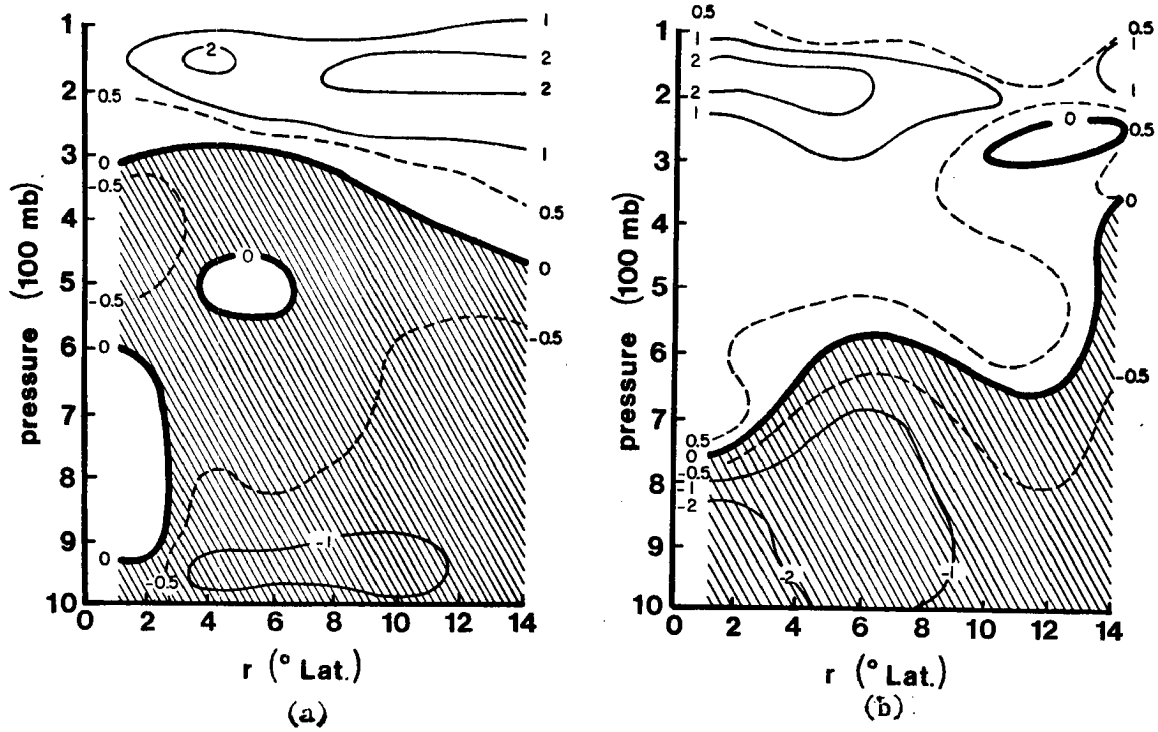

Fig. 39. Cross-section of radial wind for (a) developing (ATD2) and (b) non-developing (ATN3) tropical depressions in the northwest Atlantic.

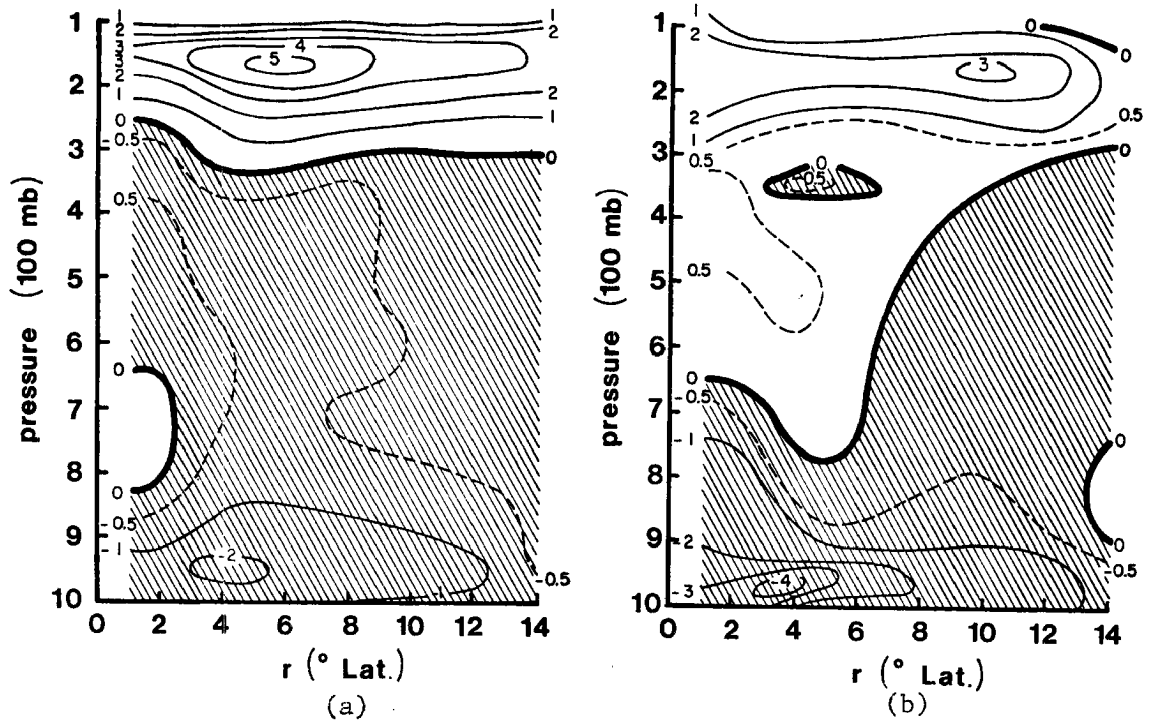

Fig. 40. Cross-section of radial wind for (a) developing (WPD3) and (b) non-developing (WPN3) tropical storms in the northwest Pacific.

the TCE is quite complicated and this observational study cannot fully address this problem. Special numerical modeling work along these lines would be highly desirable.

The importance of this radial circulation is highlighted when the horizontal transport of angular momentum is considered. As has been shown in Fig. 22a, the tangential wind increases through a very deep layer at the inner region causing the increase in middle to upper level vertical wind shear as the system intensifies. This increased wind shear will then be able to sustain a greater upper level warm core, and a subsequent lower surface pressure. Since cumulus convection is primarily a down gradient mixing process this increase of vertical wind shear should be attributed to the horizontal transport. The importance of the horizontal transport of angular momentum in tropical cyclone systems has also been discussed by Holland (1981). The point being addressed here is the importance of the deep inflow and the concentrated outflow layers for the developing cyclones. This deep inflow appears to be responsible for the increase of tangential wind through a deep layer. At the upper levels, the outward transport of tangential momentum just balances the large increase of tangential momentum due to convective transport.

Figure 41 illustrates the idealized tangential wind changes at the inner region associated with the horizontal and vertical transports (and surface frictional effect). Curve a is the assumed initial tangential wind profile and curve b is the resulting tangential wind profile after cumulus convection (or local mass recycling) if we assume that there is no net radial wind. (The differences between curves a and b at each layer have been scaled to represent the calculated TCE.) However, there

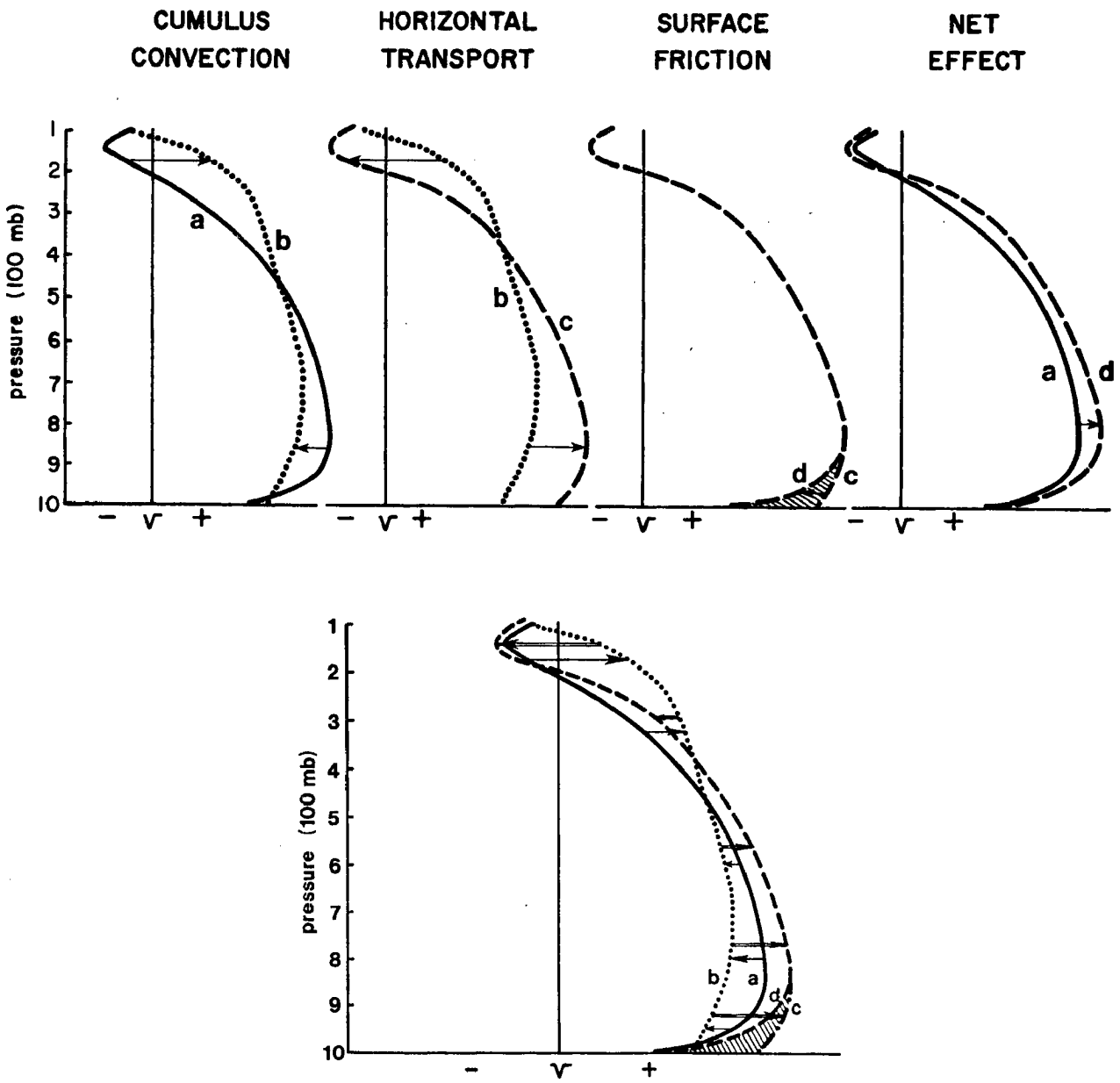

Fig. 41. Idealized diagram showing the effects of the vertical and horizontal transports of tangential wind and of the surface friction on the alteration of the tangential wind profile in the inner region of a developing tropical cyclone system. The bottom diagram is the combination of all the processes of the top diagrams. Curves a and d represent the observed initial and final tangential wind profiles for a tropical cyclone system which is undergoing development (top right diagram). Curve b is the speculated profile after cumulus convection only - (assume no radial wind). The difference between curves b and a are scaled to represent the calculated TCE profile. The horizontal transport of tangential wind due to radial circulation will change the tangential wind profile from curve b to curve c. At the same time, surface frictional effect will reduce low level tangential wind from curve c to curve d. Curve d is thus the final and stronger tangential wind profile resulting from all these effects.

is always a mean radial circulation accompanying the cumulus convection. The horizontal transport of tangential wind associated with this radial circulation will change the tangential wind profile from curve b to curve c. Along with the vertical and horizontal transport, the surface frictional effect always acts to decrease the boundary layer tangential wind from curve c to curve d. Curve d is thus the final and stronger tangential wind profile resulting from all these effects.

At the outer region, the increase of upper level anticyclonic wind (Fig. 22b) is primarily due to the concentrated outflow (Figs. 39a and 40a) which exports very large amount of absolute vorticity (which is always positive) to larger radii (Eq. 26). In the middle and lower levels, horizontal and vertical transports are relatively smaller and tend to balance each other, causing only a slight increase in tangential wind.

6. SUMMARY AND CONCLUSION

Cumulus friction (or the unresolvable part of the convective effect) can be calculated as a residual of the large scale momentum budget. Such calculations have been performed for 16 data sets corresponding to different intensity stages of tropical cyclones in the northwest Atlantic and northwest Pacific. Azimuthal averaging has been used to avoid calculating the pressure gradient term. To reduce horizontal eddy effects on the residual calculation, only the 1-5^{o} latitude radii results have been analyzed. These residual cumulus friction effects were found to exhibit the same pattern for all the developing data sets: positive at upper and lower layers and negative at levels in between. The stronger systems have a greater amplitude of cumulus friction than the weaker systems. The differences between the developing and non-developing systems were found to be consistent at each intensity stage for both ocean basins.

Cumulus friction was found to have a magnitude comparable to the mean vertical motion transport and a pattern similar to the total convective effect. Thus, any numerical modeling work which attempts to simulate tropical convective systems ought to include this cumulus friction effect. To properly include these vertical mixing influences in a numerical model one is required to develop an adequate parameterization scheme. A simple single-cloud model was developed for this purpose. This model included a single cloud updraft and three different types of downward motion. The results show that a simple relationship for the influence of cumulus convection, namely $-\partial[\omega_c(v_c-\bar{v})]/\partial p$, can be used to represent satisfactorily such cumulus vertical momentum mixing influences. In addition, the consistency between the calculated residuals

and model-diagnosed results add support to both observational and model-inferred results.

The total convective effect (TCE) was found to exhibit a negative value at the level of maximum cyclonic wind and a positive value at the primary outflow layer (or to decrease both lower level cyclonic and upper level anticyclonic winds). This leads to the conclusion that although up-gradient transport might occur under certain conditions to increase the vertical wind shear, the net influence of cumulus convection in tropical cyclones is primarily a down-gradient mixing process which acts to reduce the large scale vertical wind shear. These findings are consistent with the recent Harvard School speculations on the bulk influences of cumulus convection on large scale momentum fields (Schneider and Lindzen, 1976; Stevens et al., 1977; Shapiro, 1978; Shapiro and Stevens, 1980).

The findings of this paper do not support the Imperial College, U.K. ideas of Moncrieff and Green (1972) and Moncrieff and Miller (1976) on the possible influence of deep convection acting to increase vertical wind shear (at least in an aggregate sense) or to the hypothesis of Gray (1979) and McBride (1979) that an up-gradient transport of momentum by deep-cumulus may be an important mechanism in tropical cyclone genesis.

LIST OF SYMBOLS

[ ]	Bracket denotes grid box average
'	Prime denotes deviation from grid box average
$\overline{\quad}$	Overbar denotes azimuthal mean
C	Condensation
C_D	Drag coefficient
c	1. Speed of cyclone movement 2. As a subscript denotes cloud
cd	As a subscript denotes cloud downdraft
cuF_θ	Cumulus friction (tangential component)
D_n	Fraction of total downward motion in form of nth kind of downdraft
d	As a subscript denotes downward motion
E	Evaporation
E_{sfc}	Surface evaporation
e	As a subscript denotes environmental cloud free area
F_θ	Subgrid scale effect (tangential component)
f	Coriolis parameter
f_o	Coriolis parameter at the storm center
g	1. Gravity 2. As a subscript denotes environmental gentle subsidence
k	As a subscript denotes vertical levels. k = 0 at the surface
M_a	Absolute angular momentum
m	As a subscript denotes mean vertical mass flux
md	As a subscript denotes meso-scale downdrafts
n	As a subscript denotes nth kind of downdrafts
p	Pressure, vertical axis
Q	Moisture flux

LIST OF SYMBOLS (cont'd)

q	Mixing ratio
q_s	Saturation mixing ratio
R	Condensation to rain by all the upward motions
r	1. Radius, radial axis 2. As a subscript denotes local mass recycling
SF_θ	Surface friction (tangential component)
TCE	Total convective effect (tangential component)
u	1. Radial component of momentum, radial wind 2. As a subscript denotes upward motion
v	Tangential component of momentum, tangential wind
x_p	Sub-grid scale pressure gradient force
θ	1. azimuth, measured counterclockwise from the north 2. as a subscript denotes tangential component
ρ	Density
σ	Fraction of total area covered by cloud
τ_h	Stress at the top of mixing layer (=0)
τ_o	Surface stress
Φ	Geopotential height
ω	Vertical p velocity or vertical mass flux (mb/d)
ζ_a	Absolute vorticity

ACKNOWLEDGEMENTS

The author gratefully acknowledges the continuous support, guidance and encouragement of his advisor, Professor William M. Gray. In addition, the author would like to thank his colleagues Johnny Chan, Greg Holland, Geoff Love and Robert Merrill for their comments on this manuscript. The author is also appreciative of the helpful comments by Professors W. H. Schubert, D. E. Stevens, R. H. Johnson, and Dr. W. A. Fingerhut. The technical assistance of manuscript preparation by Ms. Barbara Brumit and Ms. Cindy Schrandt is also greatfully acknowledged. This research is funded by ONR contract grant No. N00014-C-0793.

REFERENCES

Arnold, C. P., 1977: Tropical cyclone cloud and intensity relationships. Dept. of Atmos. Sci. Paper No. 277, Colo. State Univ., Ft. Collins, CO, 154 pp.

Austin, P. M. and R. A. Houze, 1973: A technique for computing vertical transports by precipitating cumuli. J. Atmos. Sci., 30, 1100-1111.

Betts, A. K., R. W. Grover and W. M. Moncrieff, 1976: Structure and motion of tropical squall-lines over Venezuela. Quart. J. Roy. Meteor. Soc., 102, 395-404.

Cho, H. R., L. Cheng and R. M. Bloxam, 1979: The representation of cumulus cloud effects in the large-scale vorticity equation. J. Atmos. Sci., 36, 127-139.

Eliassen, A., 1952: Slow thermally or frictionally controlled meridional circulation in a circular vortex. Astrophys. Norv., 5, No. 2, 60 pp.

Fingerhut, W. A., 1982: Tropical cyclone genesis - numerical modeling inferences. Dept. of Atmos. Sci. Paper, Colo. State Univ., Ft. Collins, CO, 155 pp.

Frank, W. M., 1976: The structure and energetics of the tropical cyclone. Dept. of Atmos. Sci. Paper No. 258, Colo. State Univ., Ft. Collins, CO, 180 pp.

Frank, W. M., 1977a: The structure and energetics of the tropical cyclone, Part I: Storm structure. Mon. Wea. Rev., 105, 1119-1135.

Frank, W. M., 1977b: The structure and energetics of the tropical cyclone, Part II: Dynamics and energetics. Mon. Wea. Rev., 105, 1136-1150.

Frank, W. M., 1977c: Convective fluxes in tropical cyclones. J. Atmos. Sci., 34, 1554-1568.

Fujita, T. T. and P. G. Black, 1970: In-and outflow field of Hurricane Debbie as revealed by echo and cloud velocities from airborne radar and ATS-III pictures. SMRP Research Paper No. 93, Dept. of the Geophys. Sci., The Univ. of Chicago, 354-358.

Garratt, J. R., 1977: Review of drag coefficients over oceans and continents. Mon. Wea. Rev., 105, 7, 915-929.

Gray, W. M., 1967: The mutual variation of wind, shear and baroclinicity in the cumulus convective atmosphere of the hurricane. Mon. Wea. Rev., 95, 55-74.

Gray, W. M., 1973: Cumulus convection and large scale circulations, I: Broadscale and mesoscale considerations. Mon. Wea. Rev., 101, 839-855.

Gray, W. M., 1979: Hurricanes: their formation, structure and likely role in the tropical circulation. Supplement to Meteorology Over the Tropical Oceans. Published by RMS, James Glaisher House, Grenville Place, Bracknell, Berkshire, RG 12 1BX, D. B. Shaw, ed., 155-218.

Gray, W. M., 1981: Recent advances in tropical cyclone research from rawinsonde composite analysis. Paper prepared for the WMO Committee of Atmospheric Science, Geneva, Switzerland, 407 pp.

Gray, W. M., E. Buzzell, G. Burton and other project personnel, 1982: Tropical cyclone and related meteorological data sets available at CSU and their utilization. Dept. of Atmos. Sci. Report, Colo. State Univ., Ft. Collins, CO, 186 pp.

Hack, J. J. and W. H. Schubert, 1980: The role of convective scale processes in tropical cyclone development. Dept. of Atmos. Sci. Paper No. 330, Colo. State Univ., Ft. Collins, CO, 206 pp.

Holland, G. J., 1981: Angular momentum budget in tropical cyclones. Dept. of Atmos. Sci. M. S. Thesis, Colo. State Univ., Ft. Collins, CO, 74 pp.

Johnson, R. H., 1976: The role of convective-scale precipitation downdrafts in cumulus and synoptic scale interactions. J. Atmos. Sci., 33, 1890-1910.

Johnson, R. H., 1980: Diagnosis of convective and meso-scale motions during Phase III of GATE. J. Atmos. Sci., 37, 733-753.

Lopez, R. E., 1973: Cumulus convection and larger scale circulations, II: Cumulus and mesoscale interaction. Mon. Wea. Rev., 101, 856-870.

McBride, J. L., 1979: Observational analysis of tropical cyclone formation. Dept. of Atmos. Sci. Paper No. 308, Colo. State Univ., Ft. Collins, CO, 230 pp.

McBride, J. L., 1981: Observational analysis of tropical cyclone formation. Part I: Basic description of data sets. J. Atmos. Sci., 38, 1117- 1131.

McBride, J. L. and R. Zehr, 1981: Observational analysis of tropical cyclone formation. Part II: Comparison of non-developing vs. developing systems. J. Atmos. Sci., 38, 1132-1151.

Miller, B. I., 1958: Rainfall rates in Florida hurricanes. Mon. Wea. Rev., 86, 258-264.

Moncrieff, M. W. and J. S. A. Green, 1972: The propagation and transfer properties of steady convective overturning in shear. Quart. J. Roy. Meteor. Soc., 98, 336-352.

Moncrieff, M. W. and M. J. Miller, 1976: The dynamics and simulation of tropical cumulus and squall line. Quart. J. Roy. Meteor. Soc., 102, 373-394.

Neal, A. B. and G. J. Holland, et al., 1978: Australian tropical cyclone forecasting manual. Bureau of Meteorology, Australia.

Nunez, E., 1982: Tropical cyclone structure and intensity change. Dept. of Atmos. Sci. Paper, Colo. State Univ., Ft. Collins, CO, 192 pp.

Reed, R. J. and E. E. Recker, 1971: Structure and properties of synoptic-scale wave disturbances in the equatorial western Pacific. J. Atmos. Sci., 28, 1117-1133.

Reed, R. J. and R. H. Johnson, 1974: The vorticity budget of synoptic scale wave disturbances in the tropical western Pacific. J. Atmos. Sci., 31, 1784-1790.

Reed, R. J., D. Norquist and E. E. Recker, 1977: The structure and properties of African wave disturbances as observed during Phase III of GATE. Mon. Wea. Rev., 105, 317-333.

Roll, H. U., 1965: Physics of the maritime atmosphere. Academic Press, New York, NY, 426 pp.

Saucier, W. J., 1955: Principles of meteorological analysis. The University of Chicago Press.

Schneider, E. K. and R. S. Lindzen, 1976: A discussion of the parameterization of momentum exchange by cumulus convection. J. Geophys. Res., 81, 3158-3160.

Shapiro, L. J., 1978: The vorticity budget of a composite African tropical wave disturbance. Mon. Wea. Rev., 106, 806-817.

Shapiro, L. J. and D. E. Stevens, 1980: Parameterization of convective effects on the momentum and vorticity budgets of synoptic-scale Atlantic tropical waves. Mon. Wea. Rev., 108, 1816-1826.

Schubert, W. H., J. J. Hack, P. L. Silva Dias and S. R. Fulton, 1980: Geostrophic adjustment in an axisymmetric vortex. J. Atmos. Sci., 37, 1464-1484.

Schubert, W. H. and J. J. Hack, 1981: Inertial stability and tropical cyclone development. To be published in J. Atmos. Sci.

Silva Dias, P. L. and W. H. Schubert, 1979: The dynamics of equatorial mass-flow adjustment. Dept. of Atmos. Sci. Paper No. 312, Colo. State Univ., Ft. Colllins, CO, 203 pp.

Stevens, D. E., 1979: Vorticity, momentum and divergence budgets of synoptic-scale wave disturbances in the tropical eastern Atlantic. Mon. Wea. Rev., 107, 535-550.

Stevens, D. E., R. S. Lindzen and L. J. Shapiro, 1977: A new model of tropical waves incorporating momentum mixing by cumulus convection. Dynamics of Atmospheres and Oceans. Elsevier Scientific Publishing Company, Amsterdam, 365-425.

Thompson, R. M., S. W. Payne, E. E. Recker and R. J. Reed, 1979: Structure and properties of synoptic-scale wave disturbances in the intertropical convergence zone of the eastern Atlantic. J. Atmos. Sci., 36, 53-72.

Williams, K. T. and W. M. Gray, 1973: Statistical analysis of satellite observed cloud clusters in the western north Pacific. Tellus, 25, 178-201.

Yanai, M., S. Esbensen and J. H. Chu, 1973: Determination of bulk properties of tropical cloud clusters from large-scale heat and moisture budgets. J. Atmos. Sci., 30, 611-627.

Zipser, E. J., 1977: Mesoscale and convective scale downdrafts as distinct components of squall-line circulation. Mon. Wea. Rev., 105, 1568-1589.

W. M. GRAY'S FEDERALLY SUPPORTED RESEARCH PROJECT REPORTS SINCE 1967

CSU Dept. of Atmos. Sci. Report No.	Report Title, Author, Date, Agency Support
104	The Mutual Variation of Wind, Shear and Baroclinicity in the Cumulus Convective Atmosphere of the Hurricane (69 pp.). W. M. Gray. February 1967. NSF Support.
114	Global View of the Origin of Tropical Disturbances and Storms (105 pp.). W. M. Gray. October 1967. NSF Support.
116	A Statistical Study of the Frictional Wind Veering in the Planetary Boundary Layer (57 pp.). B. Mendenhall. December 1967. NSF and ESSA Support.
124	Investigation of the Importance of Cumulus Convection and Ventilation in Early Tropical Storm Development (88 pp.). R. Lopez. June 1968. ESSA Satellite Lab. Support.
Unnumbered	Role of Angular Momentum Transports in Tropical Storm Dissipation over Tropical Oceans (46 pp.). R. F. Wachtmann. December 1968. NSF and ESSA Support.
Unnumbered	Monthly Climatological Wind Fields Associated with Tropical Storm Genesis in the West Indies (34 pp.). J. W. Sartor. December 1968. NSF Support.
140	Characteristics of the Tornado Environment as Deduced from Proximity Soundings (55 pp.). T. G. Wills. June 1969. NOAA and NSF Support.
161	Statistical Analysis of Trade Wind Cloud Clusters of the Western North Pacific (80 pp.). K. Williams. June 1970. ESSA Satellite Lab. Support.
---	A Climatology of Tropical Cyclones and Disturbances of the Western Pacific with a Suggested Theory for Their Genesis/ Maintenance. W. M. Gray. NAVWEARSCHFAC Tech. Paper No. 19-70 (225 pp.). November 1970. (Available from US Navy, Monterey, CA). US Navy Support.
179	A diagnostic Study of the Planetary Boundary Layer over the Oceans (95 pp.). W. M. Gray. February 1972. Navy and NSF Support.
182	The Structure and Dynamics of the Hurricane's Inner Core Area (105 pp.). D. J. Shea. April 1972. NOAA and NSF Support.
188	Cumulus Convection and Larger-scale Circulation, Part I: A Parameteric Model of Cumulus Convection (100 pp.). R. E. Lopez. June 1972. NSF Support.

CSU Dept. of Atmos. Sci. Report No.	Report Title, Author, Date, Agency Support
189	Cumulus Convection and Larger-scale Circulations, Part II: Cumulus and Meso-scale Interactions (63 pp.). R. E. Lopez. June 1972. NSF Support.
190	Cumulus Convection and Larger-scale Circulations, Part III: Broadscale and Meso-scale Considerations (80 pp.). W. M. Gray. July 1972. NOAA-NESS Support.
195	Characteristics of Carbon Black Dust as a Tropospheric Heat Source for Weather Modification (55 pp.). W. M. Frank. January 1973. NSF Support.
196	Feasibility of Beneficial Hurricane Modification by Carbon Black Seeding (130 pp.). W. M. Gray. April 1973. NOAA Support.
199	Variability of Planetary Boundary Layer Winds (157 pp.). L. R. Hoxit. May 1973. NSF Support.
200	Hurricane Spawned Tornadoes (57 pp.). D. J. Novlan. May 1973. NOAA and NSF Support.
212	A Study of Tornado Proximity Data and an Observationally Derived Model of Tornado Genesis (101 pp.). R. Maddox. November 1973. NOAA Support.
219	Analysis of Satellite Observed Tropical Cloud Clusters (91 pp.). E. Ruprecht and W. M. Gray. May 1974. NOAA-NESS Support.
224	Precipitation Characteristics in the Northeast Brazil Dry Region (56 pp.). R. P. L. Ramos. May 1974. NSF Support.
225	Weather Modification through Carbon Dust Absorption of Solar Energy (190 pp.). W. M. Gray, W. M. Frank, M. L. Corrin, and C. A. Stokes. July 1974.
234	Tropical Cyclone Genesis (121 pp.). W. M. Gray. March 1975. NSF Support.
---	Tropical Cyclone Genesis in the Western North Pacific (66 pp.). W. M. Gray. March 1975. US Navy Environmental Prediction Research Facility Report. Tech. Paper No. 16-75. (Available from the US Navy, Monterey, CA). Navy Support.
241	Tropical Cyclone Motion and Surrounding Parameter Relationships (105 pp.). J. E. George. December 1975. NOAA Support.

CSU Dept. of Atmos. Sci. Report No.	Report Title, Author, Date, Agency Support
243	Diurnal Variation of Oceanic Deep Cumulus Convection. Paper I: Observational Evidence, Paper II: Physical Hypothesis (106 pp.). R. W. Jacobson, Jr. and W. M. Gray. February 1976. NOAA-NESS Support.
257	Data Summary of NOAA's Hurricane Inner-Core Radial Leg Flight Penetrations 1957-1967, and 1969 (245 pp.). W. M. Gray and D. J. Shea. October 1976. NSF and NOAA Support.
258	The Structure and Energetics of the Tropical Cyclone (180 pp.). W. M. Frank. October 1976. NOAA-NHEML, NOAA-NESS and NSF Support.
259	Typhoon Genesis and Pre-typhoon Cloud Clusters (79 pp.). R. M. Zehr. November 1976. NSF Support.
Unnumbered	Severe Thunderstorm Wind Gusts (81 pp.). G. W. Walters. December 1976. NSF Support.
262	Diurnal Variation of the Tropospheric Energy Budget (141 pp.). G. S. Foltz. November 1976. NSF Support.
274	Comparison of Developing and Non-developing Tropical Disturbances (81 pp.). S. L. Erickson. July 1977. US Army Support.
77-01	Tropical Cyclone Research by Data Compositing (70 pp.). W. M. Gray and W. M. Frank. July 1977. Navy Support.
277	Tropical Cyclone Cloud and Intensity Relationships (154 pp.). C. P. Arnold. November 1977. US Army and NHEML Support.
297	Diagnostic Analyses of the GATE A/B-scale Area at Individual Time Periods (102 pp.). W. M. Frank. November 1978. NSF Support.
298	Diurnal Variability in the GATE Region (80 pp.). J. M. Dewart. November 1978. NSF Support.
299	Mass Divergence in Tropical Weather Systems, Paper I: Diurnal Variation; Paper II: Large-scale Controls on Convection (109 pp.). J. L. McBride and W. M. Gray. November 1978. NOAA-NHEML Support.
78-01	New Results of Tropical Cyclone Research from Observational Analysis (108 pp.). W. M. Gray and W. M. Frank. June 1978. Navy Support.

CSU Dept. of Atmos. Sci. Report No.	Report Title, Author, Date, Agency Support
305	Convection Induced Temperature Change in GATE (128 pp.). P. G. Grube. February 1979. NSF Support.
308	Observational Analysis of Tropical Cyclone Formation (230 pp.). J. L. McBride. April 1979. NOAA-NHEML, NSF and NEPRF Support.
333	Tropical Cyclone Intensity Change - A Quantitative Forecasting Scheme. K. M. Dropco. May 1981. NOAA Support.
340	The Role of the General Circulation in Tropical Cyclone Genesis (230 pp.). Geoff Love. April 1982. NSF Support.
341	Cumulus Momentum Transports in Tropical Cyclones. Cheng Shang Lee. May 1982. ONR Support.
343	Tropical Cyclone Movement and Surrounding Flow Relationships (68 pp.). Johnny C. L. Chan and William M. Gray. May 1982. ONR Support
346	Environmental Circulations Associated with Tropical Cyclones Experiencing Fast, Slow, and Looping Motions. Jianmin Xu and William M. Gray. May 1982. ONR Support.
348	Tropical Cyclone Motion: Environmental Interaction Plus A Beta Effect. Greg. J. Holland. May 1982. ONR Support.
---	Tropical Cyclone and Related Meteorological Data Sets Available at CSU and Their Utilization. W. M. Gray, E. Buzzell, G. Burton, G. Holland and Other Project Personnel. February 1982. NSF, ONR, NOAA, NEPRF Support.